PLOS PATHOGENS

RESEARCH ARTICLE

Glycan heterogeneity as a cause of the persistent fraction in HIV-1 neutralization

Rajesh P. Ringe[1¤a], Philippe Colin[1¤b], Gabriel Ozorowski[2], Joel D. Allen[3], Anila Yasmeen[1], Gemma E. Seabright[3], Jeong Hyun Lee[2¤c], Aleksandar Antanasijevic[2¤d], Kimmo Rantalainen[2¤e], Thomas Ketas[1], John P. Moore[1], Andrew B. Ward[2¤c]*, Max Crispin[3]*, P. J. Klasse[1]*

1 Department of Microbiology and Immunology, Weill Cornell Medicine, Cornell University, New York, New York, United States of America, **2** Department of Integrative Structural and Computational Biology, The Scripps Research Institute, La Jolla, California, United States of America, **3** School of Biological Sciences, University of Southampton, Southampton, United Kingdom

¤a Current address: Virology Unit, Institute of Microbial Technology, Council of Scientific and Industrial Research (CSIR), Chandigarh, India
¤b Current address: Toulouse Institute for Infectious and Inflammatory Diseases, Infinity, Université de Toulouse, CNRS, INSERM, UPS, Toulouse, France
¤c Current address: Consortium for HIV/AIDS Vaccine Development (CHAVD), International AIDS Vaccine Initiative (IAVI), The Scripps Research Institute, La Jolla, California, United States of America
¤d Current address: Global Health Institute, École Polytechnique Fédérale de Lausanne, Lausanne, Switzerland
¤e Current address: Department of Immunology and Microbiology, The Scripps Research Institute, La Jolla, California, United States of America
* andrew@scripps.edu (ABW); max.crispin@soton.ac.uk (MC); pek2003@med.cornell.edu (PJK)

Citation: Ringe RP, Colin P, Ozorowski G, Allen JD, Yasmeen A, Seabright GE, et al. (2023) Glycan heterogeneity as a cause of the persistent fraction in HIV-1 neutralization. PLoS Pathog 19(10): e1011601. https://doi.org/10.1371/journal.ppat.1011601

Editor: Daniel C. Douek, Vaccine Research Center, UNITED STATES

Received: August 7, 2023

Accepted: October 5, 2023

Published: October 30, 2023

Data Availability Statement: DATA AVAILABILITY The CZA97.012+3BNC117 cryo-EM map and model have been deposited to the Electron Microscopy Data Bank under accession code EMD-40088 and the Protein Data Bank under accession code 8gje, respectively.

Funding: We are grateful for the following funding of this study: The National Institute of Allergy and Infectious Diseases of the National Institutes of Health R01 AI036082 (PJK and JPM), P01 AI110657 (PJK, JPM, ABW), and The International

Abstract

Neutralizing antibodies (NAbs) to multiple epitopes on the HIV-1-envelope glycoprotein (Env) have been isolated from infected persons. The potency of NAbs is measured more often than the size of the persistent fraction *of* infectivity at maximum neutralization, which may also influence preventive efficacy of active or passive immunization and the therapeutic outcome of the latter. Many NAbs neutralize HIV-1 CZA97.012, a clone of a Clade-C isolate, to ~100%. But here NAb PGT151, directed to a fusion-peptide epitope, left a persistent fraction of 15%. NAb PGT145, ligating the Env-trimer apex, left no detectable persistent fraction. The divergence in persistent fractions was further analyzed by depletion of pseudoviral populations of the most PGT151- and PGT145-reactive virions. Thereby, neutralization by the non-depleting NAb increased, whereas neutralization by the depleting NAb decreased. Furthermore, depletion by PGT151 increased sensitivity to autologous neutralization by sera from rabbits immunized with soluble native-like CZA97.012 trimer: substantial persistent fractions were reduced. NAbs in these sera target epitopes comprising residue D411 at the V4-β19 transition in a defect of the glycan shield on CZA97.012 Env. NAb binding to affinity-fractionated soluble native-like CZA97.012 trimer differed commensurately with neutralization in analyses by ELISA and surface plasmon resonance. Glycan differences between PGT151- and PGT145-purified trimer fractions were then demonstrated by mass spectrometry, providing one explanation for the differential antigenicity. These differences were interpreted in relation to a new structure at 3.4-Å resolution of the soluble CZA97.012 trimer determined by cryo-electron microscopy. The trimer adopted a closed conformation,

AIDS Vaccine Initiative (IAVI) through grant INV-008352/OPP1153692 funded by the Bill and Melinda Gates Foundation (M.C.). The funders had no role in study design, data collection and analysis, decision to publish, or preparation of the manuscript.

Competing interests: We declare that we have no competing interests.

refuting apex opening as the cause of reduced PGT145 binding to the PGT151-purified form. The evidence suggests that differences in binding and neutralization after trimer purification or pseudovirus depletion with PGT145 or PGT151 are caused by variation in glycosylation, and that some glycan variants affect antigenicity through direct effects on antibody contacts, whereas others act allosterically.

Author summary

Neutralizing antibodies block the entry of HIV-1 into cells and protect against HIV-1 infection in animal models. Therefore, vaccination aims to elicit antibodies that potently neutralize most HIV-1 variants. Such antibodies suppress virus levels when given to HIV-1-infected patients. Their potency is often measured as the concentration that gives 50% or 80% neutralization. But higher degrees of neutralization are needed to protect an organism from infection. And for some antibodies a ceiling is reached, so that even with increasing concentration a constant fraction of infectious virus persists. We studied the carbohydrate moieties on the envelope glycoprotein, which is the sole target for neutralizing antibodies, of one HIV-1 isolate of the most widespread subtype, Clade C, prevalent in Africa and Asia. We show how differences in carbohydrates can contribute to persistent infectivity, because distinct carbohydrates fit different antibodies. With a new three-dimensional structure of the entry-mediating protein from the Clade-C isolate, we illustrate that some carbohydrate differences occur exactly where the antibodies bind, whereas others are located elsewhere and can act indirectly. When we combined two neutralizing antibodies, the persistent infectivity shrank. Our results reinforce the need for multiple specificities of neutralizing antibodies in prevention and therapy.

Introduction

Neutralizing antibodies (NAbs) are the best correlate of protection against several viral infections [1–7]. Broadly active NAbs (bNAbs) protect against HIV-1 acquisition in animal models, but eliciting them through active immunization with their sole target, the viral envelope glycoprotein (Env), has proved elusive [8–17]. In contrast, therapeutic passive immunization of HIV-1-infected people by the administration of bNAbs already shows promise in clinical trials [12,18–20]. And preventive passive immunization specifically blocks acquisition of isolates that are sensitive to the administered bNAb [21,22]. The current study aims to inform all these bNAb-based applications.

When bNAbs are evaluated, much focus is on their breadth of action against panels of relatively neutralization-resistant isolates and on their efficiency or *potency*, *i.e.*, the concentration of pure bNAb that gives, *e.g.*, 50% or 80% neutralization. Arguably, however, their *efficacy*, *i.e.*, their maximum extent of neutralization of an individual isolate can also influence their preventive and therapeutic effect. Modeling based on protection of macaques from challenges with simian-human immunodeficiency virus (SHIV) by infused bNAbs and on neutralization efficacy of these bNAbs *in vitro* suggested that, at a minimum, 98% extent of neutralization would be required to get 50% protection *in vivo* [23].

The converse of the maximum of virus neutralization, known as the persistent fraction of infectivity (PF), has a long and contentious history in virology [1,24,25]. The PF can be detected as the neutralization by NAbs at increasing concentrations reaches a maximum below

100% [1,24–26]. Generally, the persistent virus is not genetically resistant, but when propagated *de novo* and re-neutralized shows sensitivity similar to that of the original input virus [1,25–28]. Genetic heterogeneity can, however, confer relative resistance to entry inhibition [29]. Several explanations of the PF have been invoked and partly supported: aggregation of virions with or without antibodies, dissociation of NAbs, failure of NAbs to induce sufficient conformational changes, competition by host-cell receptors, ancillary membrane wrapping of some enveloped viruses, and the degree of cytoplasmic Fc-receptor interactions for some naked viruses. But no general cause is known [1,24–26,28,30–36].

PFs and low slopes of the neutralization curves have been described for various isolates of HIV-1 and SHIV in combination with bNAbs directed to several epitope clusters located all over the Env trimer: at the trimer apex, the V3-base, the outer-domain mannose patch, the CD4-binding site (CD4-bs), the fusion peptide (FP) and interface between the outer (gp120) and transmembrane (gp41) subunits, and the membrane-proximate external region of gp41 [37–49]. PFs in neutralization by bNAbs directed to the trimer apex and interface-FP have been attributed to conformational flexibility, although such effects may be the atypical features of Env derived from particular isolates [37,41].

In contrast to conformational flexibility, the exceptionally dense glycan shield on HIV-1 Env quite plausibly dominates in creating epigenetic antigenic heterogeneity, the sources of glycan diversity being variation in occupancy of potential N-linked glycosylation sites (PNGSs) and differential glycan processing [50–62]. Indeed, glycan modifications by PNGS mutagenesis, use of expression cells with defects in glycan-processing enzymes, and inhibitors of such processing have implicated glycans in modulating both the potency and efficacy of neutralization [38,39,43,45,46]. Site-specific glycan analysis of gp120 combined with structural determination of the bNAb PGT135 liganded to gp120, eluciated how neutralization efficacy can be suppressed by glycan microheterogeneity at the epitope [43,45].

Here, we sought to apply both global and site-specific glycan analyses to explain varying efficacy of neutralization by antibodies directed to other epitopes than that of PGT135. We explored whether virions harboring Env spikes with distinct antigenicities and the corresponding soluble trimer molecules could be segregated by, respectively, affinity depletion and purification. We then investigated whether neutralization, binding, and glycan analyses could corroborate antigenic heterogeneities.

As model for study, we chose Env of the genotype CZA97.012, belonging to Clade C, the globally most widespread subtype of HIV-1, which is particularly prevalent in Africa and Asia [63,64]. The clone CZA97.012, also known as 97ZA.012, was isolated from peripheral blood mononuclear cells of a 29-year-old female in South Africa and is classified as relatively neutralization-resistant, *i.e.*, of Tier-2 [63,65,66]. Native-like, soluble CZA97.012 trimer of the SOSIP design can be affinity-purified by bNAbs to quaternary-structural epitopes, including PGT151 to an FP-interface epitope and PGT145 to an apical epitope; purification with the latter, however, results in low yields [40,67–69]. We have previously linked those low yields to moderately low stoichiometry and affinity of binding of PGT145 to the CZA97.012 SOSIP.664 trimer [70]. Here, we further analyzed purification with, binding of, and neutralization by PGT145 and PGT151 in the context of CZA97.012 Env.

The PGT151-purified CZA97.012 SOSIP.664 trimer elicits autologous Tier-2 NAbs in rabbits, both in homologous prime-boosting and heterologous boosting [71,72], the autologous NAbs interacting predominantly around residue D411 in the V4-β19 transition in a hole in the glycan shield, as shown previously for the heterologous-boost sera [71]. Here, the autologous neutralization of CZA97.012 pseudovirus (PV) exhibited variable and sometimes substantial PFs, of up to 60%. Neutralization by PGT151 left a PF of 15% in but none was detected with PGT145 or 3BNC117, the latter directed to an epitope mainly overlapping the CD4bs on

one protomer but also including the base of the V3 region on an adjacent one [69,73]. CZA97.012 neutralization thus manifested a spectrum of drastically different efficacies for further dissection.

Hence, for multiple reasons we chose CZA97.012 PV and the corresponding SOSIP.664 trimer for testing glycan-based explanations for the variable PF. We confirmed that virions in PV populations have differential reactivities with specific bNAbs by partially depleting PV with PGT145- or PGT151-conjugated beads. We also compared NAb binding to the CZA97.012 SOSIP.664 trimer [67] affinity-purified by different bNAbs. We then explored differences in global and site-specific glycan content in the population of differentially bNAb-reactive trimer molecules by chromatography and mass spectrometry [51–53,56,61,62,74]. Then we interpreted the glycan effects in their oligomeric-protein context through a novel cryo-EM structure of the CZA92.012 SOSIP.664 trimer in complex with 3BNC117 [69,73]. Through the ensemble of analyses, we could thus dissect the causes of the variation in PF size. Building on these findings, we finally outline how multiple specificities of bNAbs, recognizing diverse glycoforms of Env, could beneficially be elicited in active and selected in passive immunization.

Results

The persistent fraction in CZA97.012 PV neutralization

Neutralization of CZA97.012 PV by PGT145 and PGT151 is shown in **Fig 1**. As illustrated there, neutralization potency was disconnected from neutralization efficacy. PGT151 was 51-fold more potent than PGT145 at 50% neutralization (IC_{50} values: 0.15 and 7.6 μg/ml, respectively), but less effective than PGT145, leaving a PF at 50 μg/ml of 15%. PGT145 neutralization, in contrast, asymptotically approached 100%. The two bNAbs were then combined at a ratio of 99 to 1, *i.e.*, close to their IC_{50} ratio. Under those conditions, which optimize detection of synergy in potency, the two bNAbs synergized only weakly at 50% neutralization (combination index, CI = 0.79, Loewe analysis [29,75,76]). The two bNAbs combined at a ratio of 1 to 1, were weakly antagonistic, possibly reflecting the unidirectional inhibition of PGT151 binding by PGT145 [77] (CI = 1.2). The neutralization curves for the two bNAbs crossed at 80%, yielding an IC_{80} ratio of 1 and thereby optimal sensitivity for detecting synergy at that level of neutralization. Indeed, at 80% neutralization by the combined bNAbs, the synergy was stronger for the ratio of 1 to 1 (CI = 0.52) than of 99 to 1 (CI = 0.63). The main observation, thus, is that the two bNAbs synergized most strongly in the zone close to the maximum efficacy of PGT151, the combination yielding a visibly smaller PF than did PGT151 alone (**Fig 1A**).

The degree of maximum inhibition by the individual bNAbs was too high to allow a classic Bliss analysis of synergy in extent [75,76,78]. Nor could the non-synergistic efficacy of the combination be rationally predicted, because having more than one bNAb molecule bound per trimer may be either redundant or may incrementally augment neutralization [79]. Therefore only the PFs were compared: it was 2-fold smaller for the combination at a ratio of 1 to 1 than for PGT151 alone; it was undetectable for the combination at a ratio of 99 to 1, as for PGT145 alone. Hence, combining the bNAbs enhanced the extent of neutralization but only in proportion to the effects of the constituent bNAbs.

A plausible explanation both for enhanced efficacy and for synergy in potency would be antigenic heterogeneity, the mechanism being complementary preferences for binding to distinct antigenic forms in the epitope population distributed over the virions [29]. This explanation was first explored by differential depletion of PV, as schematically outlined in **Fig 1B**.

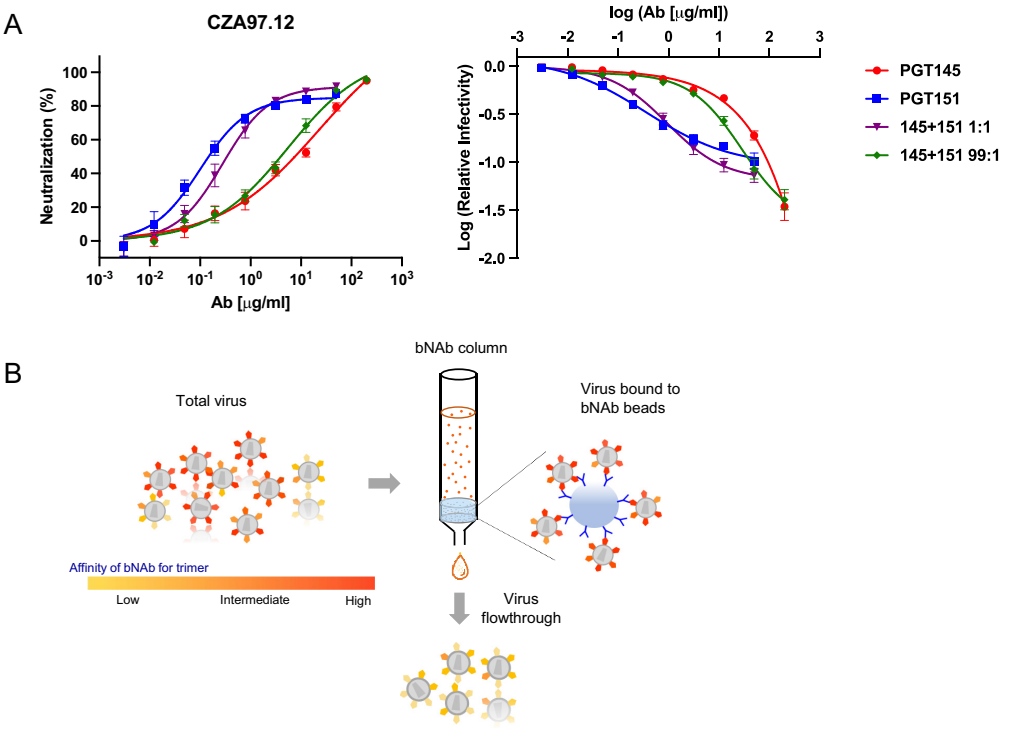

Fig 1. Neutralization and depletion of CZA97.012 PV. A. Extent of neutralization of un-depleted PV (%) in a TZM-bl assay is plotted as a function of the concentration (μg/ml) of PGT145 or PGT151 or their combined total concentration at a mixture of 1 + 1 or 99 + 1 (left). The same results are plotted as the log of infectivity relative to absence of bNAb as a function of the log of bNAb concentration, a plot that better reveals small differences in efficacy and PF (right). The data points in both diagrams are means of 13 replicates ± s.e.m. **B.** The schematic shows preferential depletion of PV particles decorated with Env that binds with high affinity to bNAbs immobilized on Sepharose beads. The unbound virions were then tested in the TZM-bl-based neutralization assay against bNAbs and sera.

https://doi.org/10.1371/journal.ppat.1011601.g001

Effects on neutralization of differential depletion of PV by bNAbs

Before the depletions, one potential contributor to the PF was ruled out: incomplete neutralization could arise from an excess of Env in high-dose inocula that would absorb NAbs, only native-like Env being relevant in the case of PGT145 and PGT151. If instead the amount of antigen is negligible in relation to the neutralizing NAb concentrations, the proportion of virus that is neutralized will remain approximately constant over a range of PV-input doses. The drop in $\log_{10}$ relative infectivity did not, in fact, vary significantly for neutralization by PGT145 or PGT151 at a constant concentration over a 2.5-$\log_{10}$ range of inoculum dose (S1 Fig). This result refutes absorption of bNAb by Env as a cause of the PF: it demonstrates that the relative neutralization in this concentration interval adhered to the percentage law of neutralization [80].

The results of the PV depletions are shown in **Figs** 2 and 3. PGT145-depleted PV was highly resistant to PGT145. Conversely, PGT151-depleted PV had drastically enhanced sensitivity to PGT145, the mock-depleted PV falling in between (Fig 2).

PGT151-depleted PV showed drastically reduced potency and efficacy of PGT151 neutralization of compared with mock-depleted PV. PGT145-depleted PV, however, differed little in PGT151 sensitivity from the mock control: the potency of PGT151 against PGT145-depleted PV was only modestly greater in the low concentration range (Fig 2). For PGT145- and mock-depleted PV, the persistent fraction of PGT151 neutralization was indistinguishable, ~20%. In contrast, for PGT151-depleted PV the PF was ~70% (Fig 2).

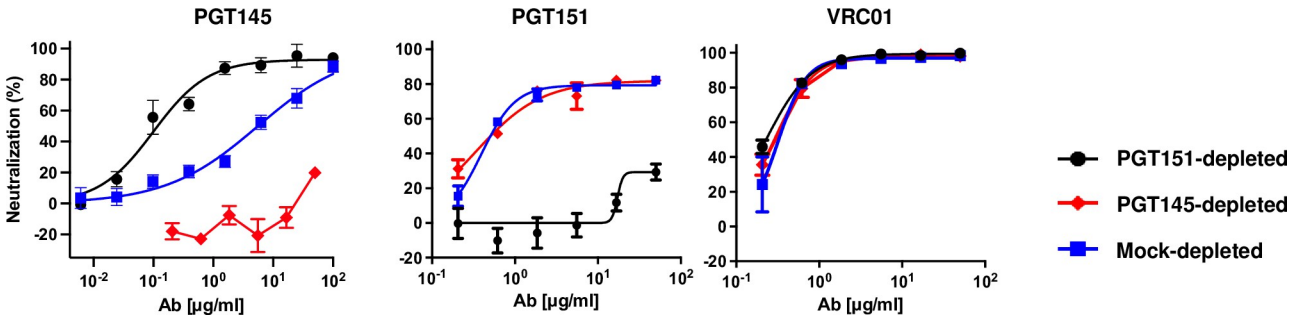

Fig 2. Neutralization of bNAb-depleted CZA97.012 PV by bNAbs. Extent of neutralization (%) is plotted as a function of NAb concentration (μg/ml). PV was first incubated with Sepharose bead-conjugated PGT145 or PGT151 or mock-depleted with control beads (color-coded legend). Unbound virions were then tested against the indicated NAb or serum in a TZM-bl neutralization assay. The data points in the diagrams are means of 2–4 replicates ± s.e.m.

https://doi.org/10.1371/journal.ppat.1011601.g002

VRC01, directed to the CD4bs [81] neutralized PGT145-, PGT151, and mock-depleted PV indistinguishably within the experimental variation (Fig 2).

The differential effects of PGT145 and PGT151 depletions were thus partly but not symmetrically reciprocal. A cogent explanation for the differences in neutralization sensitivity would be antigenic heterogeneity among the Env spikes combined with varying numbers of the antigenic forms among the virions in the PV population, as sketched in Fig 1B. Would a random, *e.g.*, binomial, distribution suffice to yield differential depletion of virions? Quite plausibly it would [79,82–84]. But more pronounced differences among virions might arise through convergence of homogeneously glycosylated trimer molecules along the secretory pathway from ER to Golgi to budding sites [82,83]. Specifically, the results suggest a more widespread antigenic heterogeneity, including greater proportions of forms virtually non-antigenic for the respective bNAb, in the PGT151 than the PGT145 epitopes on functional CZA97.012-Env spikes. Indeed, little infectivity remained for neutralization analyses after PGT145 depletion, and therefore only PGT151- and mock-depleted PVs were compared in following analyses with other antibodies.

PGT151 depletion reduced the sensitivity to two other interface-directed bNAbs, ASC202 [85] and N123-VRC34.01 [86] (Fig 3A). But it had the opposite effect of markedly enhancing the sensitivity to sera from rabbits immunized with soluble CZA97.012 SOSIP.664 trimer [72]. Indeed, one such serum, 2083, was non-neutralizing against mock-depleted PV, but upon PGT151 depletion gained neutralizing capacity, which approached 100% efficacy (Fig 3B). Autologous rabbit NAbs in such sera are known to be preferentially directed to an epitope lining a defect in the glycan shield on the CZA97.012-Env trimer around residue D411 at the V4-β19 transition [71]. Autologous NAbs in the sera collected after homologous prime and boost with CZA97 SOSIP.664 [72], were here found to be largely directed to the D411 epitope (**S3 Fig**), as shown previously only for NAbs induced by heterologous-boosts with CZA97 SOSIP.664. Notably, the serum that showed the weakest effect of PGT151 depletion, 2086, also showed the weakest effect on neutralization of the PNGS-knock-in (KI) mutation D411N: both the PGT151 depletion and the KI mutation affected mainly the potency but barely the efficacy of neutralization by serum 2086. In contrast, the neutralization by the sera 2082 and 2084 was strongly enhanced by the PGT151 depletion and also strongly reduced by the KI mutation (**Figs 3** and **S3**). In spite of the apparent interconnectedness of some of the epitopes studied, however, the KI mutation did not affect neutralization by PGT145, 2G12, VRC01, PGT151, ACS202, or N123-VRC34.01 (S2 Fig).

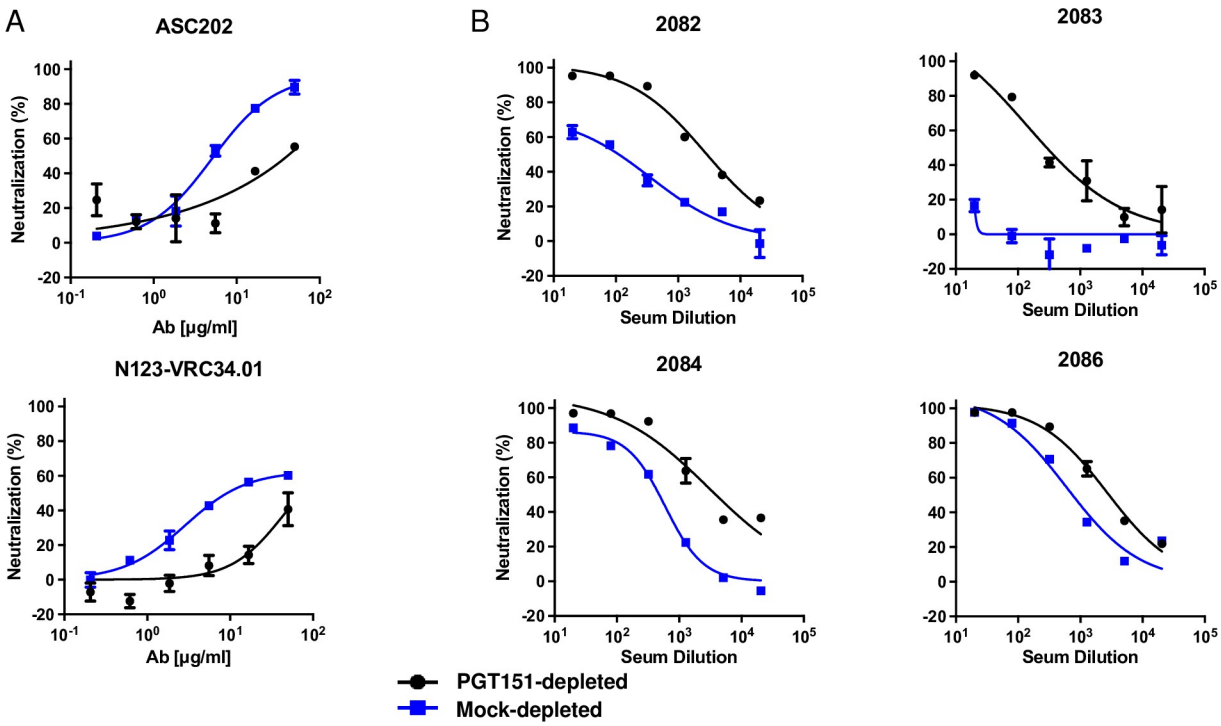

Fig 3. Neutralization of PGT151-depleted CZA97.012 PV by interface-specific bNAbs and post-immunization rabbit sera. PVs were PGT151- or mock-depleted (color-coded legend). Unbound virions were then tested against the indicated bNAb or serum in a TZM-bl assay. **A.** Extent of neutralization (%) is plotted as a function of bNAb concentration (μg/ml). **B.** Extent of neutralization (%) is plotted as a function of x-fold serum dilution. PVs were PGT151- or mock-depleted (color-coded legend). Unbound virions were then tested against the indicated bNAb or serum in a TZM-bl assay. The data points in the diagrams are means of 2 replicates ± s.e.m.

https://doi.org/10.1371/journal.ppat.1011601.g003

In conclusion, heterogeneity of the PGT145 and PGT151 epitopes is largely separable among the functional Env spikes on the virions. Lower sensitivity to PGT151 is reflected in lower sensitivity to other bNAbs directed to the FP and interface but linked to higher sensitivity for autologous NAbs directed to the glycan-hole epitope centered on D411. Plugging the latter by a PNGS-KI mutation reduced the sensitivity to the autologous NAbs but not to the tested bNAbs. Hence, we substantiated only a unidirectional connection from the PGT151 to the D411 epitope.

Effects of differential affinity purification on the antigenicity of CZA97.012 SOSIP.664 trimer

We investigated whether antigenic differences similar to those among virion-associated trimer molecules could be detected also within the population of recombinant soluble CZA97.012 SOSIP.664 molecules [70,71,87]. Field-flow fractionation in tandem with multi-angle light scattering (FFF-MALS) revealed only subtle differences in the molar masses and hydrodynamic radii of PGT145-, PGT151-, and 2G12-purified trimer molecules (Fig 4A). Any actual mass differences would be due to differential post-translational modifications, mainly in glycosylation, whereas the hydrodynamic radius could be affected by glycosylation, conformation, or aberrant folding. The latter was refuted, because trimer preparations purified by 2G12-, PGT145-, and PGT151-affinity and then size-exclusion chromatography showed indistinguishable 100% native-like structures in negative-stain electron microscopy, NS-EM (Fig 4B).

Antigenic differences associated with differential affinity purification of the CZA97.012 SOSIP.664 trimer were first explored by ELISA (Fig 5). PGT145 purification gave markedly

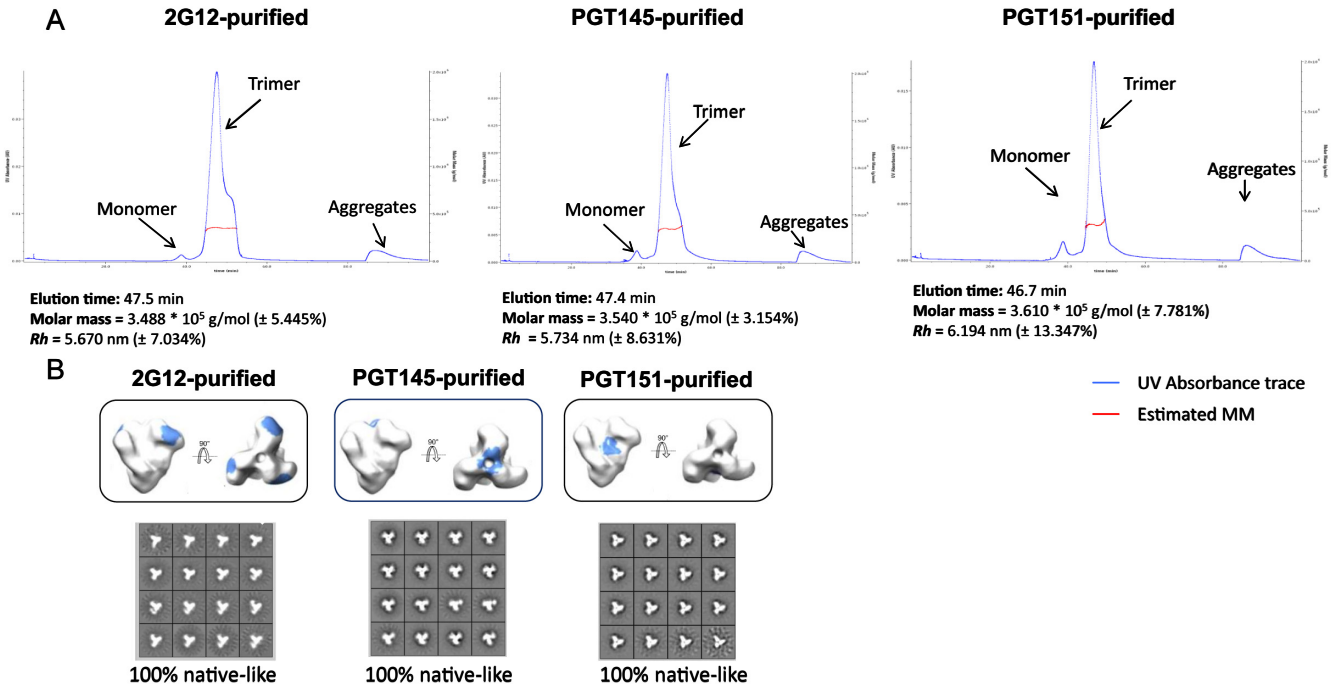

Fig 4. Molar mass and hydrodynamic radius of the CZA97.012 SOSIP.664 trimer measured by FFF-MALS. A. 2G12-, PGT145-, or PGT151- and then SEC-purified trimer was separated by FFF, and the molar mass (g/mol) and hydrodynamic radius (R_h) measured by MALS. **B.** NS-EM was performed on CZA97.012 SOSIP.664 trimer purified with three different bNAbs. CZA97.012 SOSIP.664 trimer was purified by affinity chromatography with 2G12, PGT145, or PGT151 followed by SEC. The epitopes of the three bNAbs are shown in blue on the side and top views of the trimer. 2D-class averages are shown for each purification. The calculated proportions of native-like trimer are given in % below the NS-EM images.

https://doi.org/10.1371/journal.ppat.1011601.g004

stronger binding by PGT145 itself than by PGT151 or 2G12, the latter binding being only marginally stronger than the former. 2G12 purification also gave vastly stronger binding by itself than by the other two, PGT145 binding being marginally better than PGT151. Purification with PGT151 gave strong binding by itself and barely any by PGT145, whereas 2G12 binding was intermediate. The ranking of the trimer binding by two other interface-FP-specific bNAbs, N123-VRC34.01 and ASC202, was the same as for PGT151, but their binding to the PGT145-purified trimer was stronger than that by PGT151. Together those results illustrate both similarities and specific preferences among these three bNAbs to overlapping interface-FP epitopes. Thus, Fig 5 provides strong evidence for stable antigenic heterogeneity in the expressed soluble trimer population: isoforms of the trimer with distinct presentations of each cluster of epitopes were preserved after elution from each of the purification bNAbs.

The antigenicity of differentially purified trimer was then further analyzed by SPR, which unlike ELISA reveals kinetic differences in binding and obviates exposure of some non-NAb epitopes under the ELISA conditions [48,87] (Fig 6). From apex to base, antigenic differences were detected, not just with the purification antibodies. PGT145 bound similarly to PGT145- and 2G12-purified trimer in the association phase but with markedly slower dissociation from the former than the latter. PGT145 binding to PGT151-purified trimer was reduced in both the association and dissociation phase compared with the other two purifications. The faster dissociation of PGT145 from the 2G12- and PGT151-purified trimer may explain the even lower corresponding binding by PGT145 in ELISA, in which the washes amplify loss of antibody through rapid dissociation (Fig 5). PG16, also directed to an apical trimer-specific

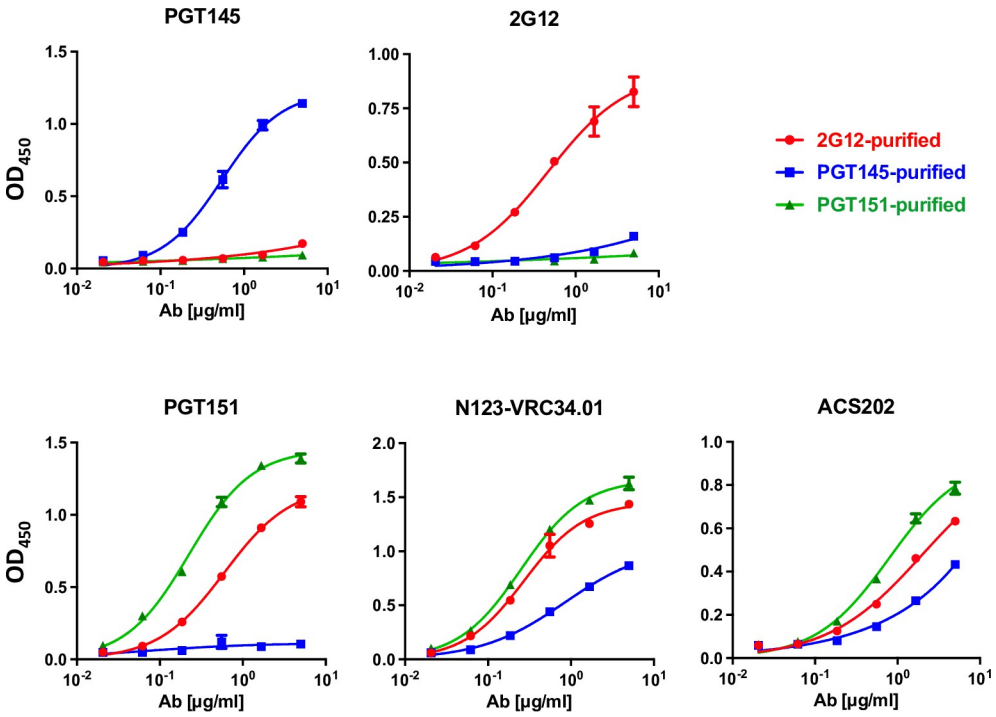

Fig 5. Analysis of bNAb binding to bNAb-fractionated SOSIP trimers by ELISA. Each diagram shows the binding of a bNAb to the CZA97.012 SOSIP.664 trimer purified with three different bNAbs (color-coded legend). The optical densities (OD_{450}) after subtraction of zero-bNAb background are depicted on the y axes as functions of the bNAb concentrations (μg/ml). The means of 2 replicates ± s.e.m. are shown.

https://doi.org/10.1371/journal.ppat.1011601.g005

epitope, differentiated even more clearly: strongest binding to PGT145-purifed, intermediate to 2G12-purified, and weakest to PGT151-purified trimer.

2G12 gave highest binding to 2G12-purified trimer, whereas its weaker binding to PG145- and PGT151-purified trimer, differed kinetically, association with and dissociation from the latter being faster (Fig 6). The rapid dissociation kinetics of 2G12 may explain its incapacity to neutralize the virus (S2 Fig). Like some other HIV-1 isolates of Clade C, CZA97.012 has both

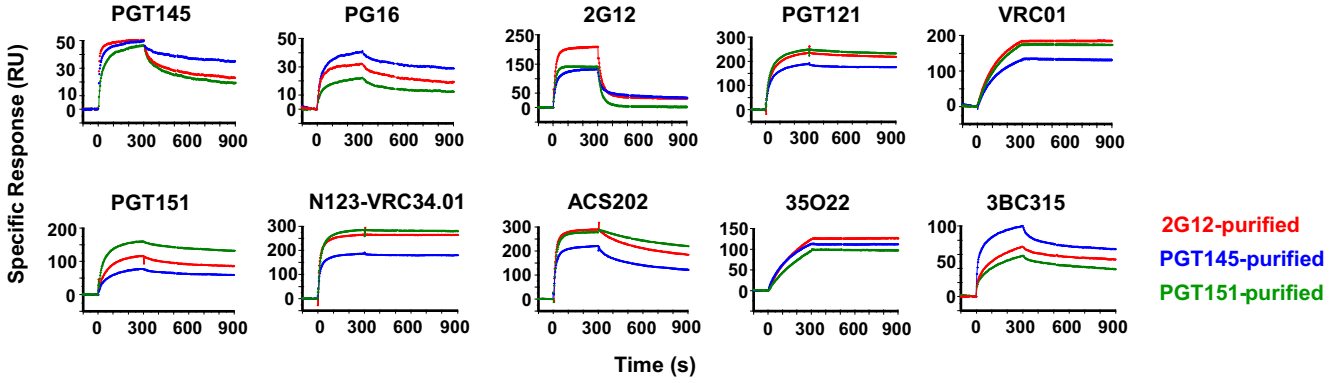

Fig 6. SPR analysis of bNAb binding to bNAb-fractionated CZA97.012 SOSIP.664 trimer. CZA97.012 SOSIP.664 trimer was purified on 2G12-, PGT145-, or PGT151-affinity columns and thereafter by SEC. Sensorgrams show binding to immobilized trimer (response units, RU) after background subtraction on the y-axis *vs*. time (s) on the x-axis. Note that the y axes have different scales in accordance with the maximum binding by each bNAb. Association was monitored for 300 s, dissociation for 600 s.

https://doi.org/10.1371/journal.ppat.1011601.g006

the N332 and N339 PNGSs but lacks the N295 and N392 ones. The net result is the unfavorable kinetics of binding and negligible neutralization by 2G12, whose binding depends on oligo-mannose glycans at these and other sites to various degrees (**S2 Fig** [67,88,89]). Although bivalency of IgG binding contributes little to HIV-1 neutralization strength because of the low Env spike density [90,91], we note that 2G12 cannot compensate at all for its high off-rate constant by ligating two Env spikes, because its domain swap creates functional monovalency [92]. Conversely, when 2G12 is immobilized onto Sepharose beads for affinity purification, the conditions for multivalent interactions do arise: up to 3 epitopes per trimer molecule may ligate 2G12 paratopes. This difference in valency explains why 2G12-affinity columns can be used for purifying CZA97.012 SOSIP.664 trimer, although it does not neutralize the corresponding PV.

PGT121 dissociated extremely slowly from all three trimer preparations but bound at a lower level to the PGT145-purified trimer than to the other two. Thus, the differentially antigenic forms of epitopes at the outer-domain mannose-patch and at the V3-base were selected by the three purification bNAbs, even though two of them engage epitopes elsewhere on the trimer.

As another example of an allosteric effect, the CD4bs-specific bNAb VRC01 showed reduced binding to PGT145-purified trimer, which may be related to the observation that a mutant trimer, CZA97.012 SOSIP.v4.2-M6-IT, shows enhanced PGT145 and reduced VRC01 binding [70]. The mutant was designed for improved PGT145 binding through multiple amino-acid changes selected from isolates with Env that binds PGT145 more strongly. Again, the reduced VRC01 binding is quite plausibly due to allosteric effects because only one change (G429R) affects a residue within the epitope of that bNAb, whose paratope contacts only the backbone of residue 429 and therefore tolerates both Gly and Arg [93].

PGT151 binding gave clearly segregated curves, highest for trimer purified with PGT151 itself, intermediate for 2G12-purified trimer, and lowest for the PGT145-purified one. Two other interface-FP bNAbs, N123-VRC34.01 and ACS202, showed reduced binding to PGT145-purified trimer. The ASC202-binding curves for the PGT151- and 2G12-purified trimers overlapped in the association phase, but ACS202 dissociated faster from 2G12- and PGT145- than PGT151-purifed trimer. A fourth interface bNAb, 35O22, which unlike the others does not make contact with the FP [49,68,85,86], differentiated less but gave yet another ranking: highest binding to 2G12-purified, intermediate to PGT145-purified, and lowest to PGT151-purified trimer. Finally, 3BC315, directed to an inter-protomeric gp41 epitope showed strongest preference for PGT145-purified, intermediate for 2G12-purified, and lowest for PGT151-purified trimer, *i.e.*, the converse of the ranking for PGT151 binding.

In summary, antigenic differences shown in **Fig 6** comprised effects on extent of binding, as well as on kinetics and thereby affinity. They were congruent in that 2G12, PGT145, and PGT151 bound best to the trimer purified with itself. Other differences were registered for epitopes that overlap those for the purification bNAbs. Yet other effects were allosteric, affecting non-overlapping epitopes. Glycosylation differences may be explanatory factors in all these cases, although other covalent modifications cannot be excluded; nor can non-covalent variations on the basis solely of these data (cf. [37]). Allosteric modulation of the antigenicity can arise through domino effects within the glycan shield through varied glycan bulk, charge, and occupancy. Differences in glycosylation may also indirectly affect side-chain and backbone angles [94,95]. We therefore next performed detailed glycan analyses.

Global and site-specific glycan content of differentially affinity-purified CZA97.012 SOSIP.664 trimer

Variation in glycosylation has been implicated in modulating both the neutralization potency and efficacy of HIV-1 [38,39,43,45,46]. Glycan heterogeneity was therefore explored in detail

as an explanation specifically of the large PF observed in neutralization of CZA97.012 by PGT151. Since glycans on Env make direct contacts with all three bNAbs used for purifying the trimers and for depleting the PV, we hypothesized that distinct glycan compositions can be detected after the respective purifications. In addition, differentially purified trimer might show distinct glycosylation at other sites that are not in contact with the paratopes, through allosteric effects.

Atypical N-linked glycan processing is abundant on HIV-1 Env. Specifically, the levels of under-processed oligomannose-type glycans are elevated on mature Env [51,53,55]. Glycan-crowded patches tend to be under-processed and hence contain fewer glycans of the complex type. These under-processed glycans form key components in epitopes for PGT145 and 2G12 [51,53,55]. The PGT151 epitope, in contrast, contains complex glycans [40,68,96]. We therefore analyzed N-glycan occupancy and processing on the CZA97.012 SOSIP.664 trimer affinity-purified with each of the three bNAbs.

We produced the trimer in a stably CZA97.012 SOSIP.664-transfected CHO-cell line, which gives high yields and quality [70]. To investigate global and site-specific differences in glycan processing among the differentially affinity-purified trimer preparations, we used hydrophilic-interaction ultra-performance liquid chromatography (HILIC-UPLC) and liquid-chromatography mass spectrometry (LC-MS).

A previously reported LC-MS-based method was employed that determines the proportions of oligomannose- and hybrid-type glycans together as one category, complex-type glycans as a second, and N-linked-glycan sequons that remain unoccupied by glycan as a third (**Fig 7** [74]). *Oligomannose-type glycans* is the collective term for the $Man_9GlcNAc_2$,

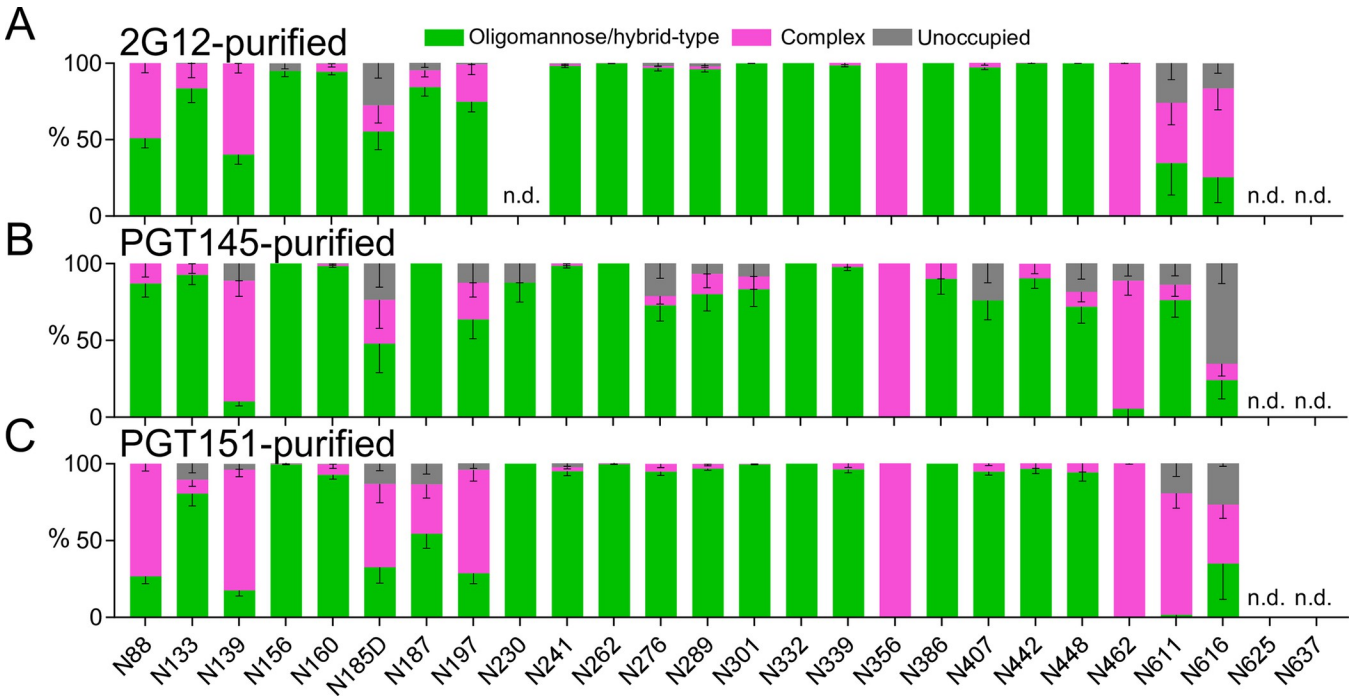

Fig 7. Site-specific glycosylation of differentially affinity-purified CZA97.012 SOSIP.664 trimer. Trimer was purified by 2G12-, PGT145-, or PGT151-affinity chromatography followed by SEC. Differentially purified trimer was analyzed by a method based on PNGase F or Endo H digestion. The bar graphs represent the relative amounts of digested glycopeptides possessing the footprints for oligo-mannose- and hybrid-type glycans together (green), complex-type glycans (magenta), and unoccupied PNGS (gray). The results were obtained by LC-MS. The error bars represent s.e.m. of all peptides detected for each site; n.d. = not detectable (which does not suggest low occupancy).

https://doi.org/10.1371/journal.ppat.1011601.g007

$Man_8GlcNAc_2$, $Man_7GlcNAc_2$, $Man_6GlcNAc_2$, and $Man_5GlcNAc_2$ moieties (where $GlcNAc_2$ denotes *N*-Acetylglucosamine). This analysis revealed an abundance of oligo-mannose- and hybrid-type glycans across gp120 and gp41 in all three purified trimer preparations, most prominently in the intrinsic mannose patch, which in the case of CZA97.012 encompasses glycans at N262, N332, N339, and N386 [55]. Furthermore, two of the key V2-apex glycan sites, N156 and N160, were also occupied almost exclusively by oligomannose- and hybrid-type glycans after all three affinity purifications. Although the variation among the differentially purified trimer populations was not drastic, the detected site-specific differences could contribute to the observed differential bNAb binding. The PGT151 epitope comprises glycans at N611 and N637, and micro-array analysis has demonstrated that PGT151 binding favors complex-type glycans [40,68]. In line with that preference, N611 on the PGT151-purified trimer was occupied by <5% oligomannose- and hybrid-type glycans, the favored complex-type glycans making up the vast majority. In contrast, on 2G12- and PGT145-purified trimer, the N611 site was largely occupied by oligomannose- and hybrid-type glycans (~40% and ~80%, respectively; **Fig 7**).

Comparing the proportions of oligomannose- or hybrid-type and complex glycan and of unoccupancy at each PNGS is informative, but it does not dissect differences in glycan compositions occurring within particular categories. One example of how the subtler subcategories matter is that the outer-domain-directed bNAb PGT135 preferentially binds to oligomannose-type glycans consisting of 8 mannose residues as opposed to 9 [45]. To investigate differences in the fine processing of oligomannose-type glycans we first used HILIC-UPLC analysis of the Endo H-released glycan pool, a method which detects global differences in oligomannose-type glycan processing (**Fig 8A**). This approach revealed similar processing of oligomannose-type glycans in 2G12- and PGT151-purified trimer, but significantly higher content of $Man_9GlcNAc_2$ in PGT145-purified trimer. Thus, the observed differences after the three affinity purifications in subsequent bNAb binding quite plausibly result from site-specific fine modifications in glycan processing. Therefore, further analyses by LC-MS were performed on intact glycopeptides. Because of markedly heterogeneous processing, the coverage of the LC-MS approach was lower, and data could not be obtained for several sites resolved in **Fig 7.** The analyses did, however, resolve the key PNGSs of the 2G12, PGT145, and PGT151 epitopes with the exception of N611 (**Fig 8B**).

$Man_9GlcNAc_2$ glycans were elevated at N332 in the 2G12-purfied trimer (**Fig 8B**). The explanation could be that 2G12 makes contacts with α1-2-mannose residues in $Man_9GlcNAc_2$ at N332 and so enriches that glycoform in the trimer population [88,89,97]. $Man_9GlcNAc_2$ glycans were also elevated in the surrounding glycans (N241, N262, N289, N363, N386, N448) but not at N339, which is a 2G12 epitope component. Since CZA97.012 lacks the PNGSs N295 and N392, which form the primary binding site in the 2G12-BG505 SOSIP.664 complex for which the structure was determined [88,97], maybe some glycans that are at the periphery of the epitope on BG505 Env instead make direct paratope contact in the CZA97.012 context. That would explain why the preferred $Man_9GlcNAc_2$ glycans were elevated at those PNGSs in addition to N332. But PGT151-purified trimer also had $Man_9GlcNAc_2$ elevations at these sites relative to the trimer purified by PGT145. Hence, an alternative explanation for the differences could be that the $Man_9GlcNAc_2$ glycans in and around the 2G12 epitope perturb the apex. Indeed, at several sites in the intrinsic mannose patch on the outer domain of gp120 PGT145-purified trimer had the lowest content of $Man_9GlcNAc_2$, although overall it had the highest (**Fig 8**). Furthermore, PGT145-purified trimer had significantly higher $Man_5GlcNAc_2$ and $Man_6GlcNAc_2$ content than the other two preparations at N339: the smaller oligomannose-type glycans could favorably affect the positioning of apical residues composing the

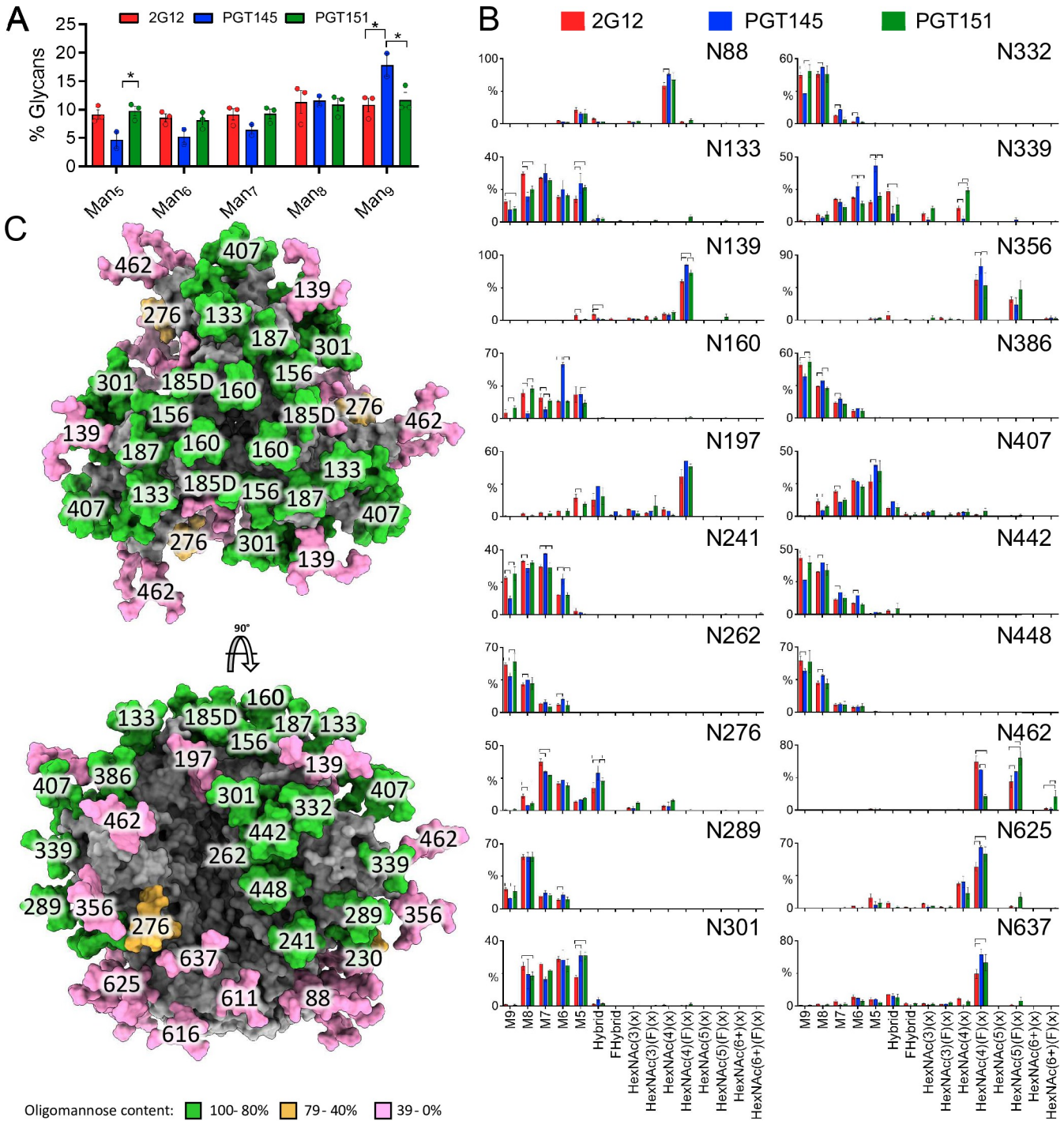

Fig 8. Global and site-specific fine glycan-type determination. A. HILIC-UPLC analysis of Endo H-released and fluorescently labeled N-glycans from CZA97.012 SOSIP.664 trimer purified by 2G12, PGT145, or PGT151 and then by SEC. The bar graphs represent the abundance of each oligomannose-type glycan as listed on the category axis. The percentage on the y axis is proportion of each oligomannose-type glycan out of the total, *i.e.*, PNGase F-released, glycan pool. **B.** CZA97.012 SOSIP.664 trimer was 2G12-, PGT145- or PGT151- and then SEC-purified. Site-specific glycan content was determined by LC-MS on intact glycopeptides. The proportion of each type of glycan is depicted on the y-axes (%), the glycan type on the horizontal category axis. Error bars show s.e.m. for 2 independent MS analyses. Significant differences within pairs of purified trimer preparations ($p<0.05$, t-test) are bracketed. **C.** Glycosylated model of a HIV-1 Env trimer (truncated C-terminally of residue 664), based on the site-specific glycan data for 2G12-purified material. The predominant glycan composition determined through the analysis displayed in panel B was modelled onto the trimer structure obtained by Cryo-EM of CZA97.012 SOSIP.664 in complex with Fab 3BNC117 and reported in this study (EMD-40088 and PDB 8gje). Where a site was not resolved by LC-MS, a representative glycan consisting of $Man_5GlcNAc_2$ was used instead. Individual glycan sites are coloured according to the abundance of oligomannose-type glycans at each site, as shown in the key.

https://doi.org/10.1371/journal.ppat.1011601.g008

PGT145 epitope, which overlie the V3 base and adjacent residues. In contrast, complex glycans at N339 were exclusively detected on 2G12- and PGT151-purified forms of trimer (Fig 8B).

The most prominent difference occurred at N160, which showed significantly more abundant $Man_6GlcNAc_2$ after purification with PGT145 than with 2G12 or PGT151 (Fig 8B). The abundance of $Man_6GlcNAc_2$ agrees with a previous structural study of PGT145 binding to the BG505 SOSIP.664 trimer, which showed that bulky glycans at that site would clash with the antibody [69]. Indeed, the density resolved for the N160 glycan in that cryo-EM study agrees with the size of $Man_6GlcNAc_2$, and its core GlcNAc moiety makes contact with the backbone of the descending strand of HCDR3 of the PGT145 Fab; its D1 arm intercalates between HCDR3 and HCDR2, while making polar contacts with the highly conserved residue H52a of the latter region [69].

Notably, the N637 glycan, integral to the PGT151 epitope, showed a significant elevation in glycans containing four N-acetylhexosamines with fucose, which typically corresponds to fucosylated biantennary glycans (HexNac(4)(F)(x)), on both PGT145- and PGT151- compared with 2G12-purified trimer (Fig 8B). This type of glycan may favor PGT151 binding but its presence does not explain the antigenic segregation of PGT151- and PGT145-purified trimer populations.

In addition, however, numerous significant differences in precise glycan type among the three differentially purified trimer preparations occurred at PNGSs not intimately involved in any of three bNAb epitopes (Fig 8B). These differences can be explained by extensive indirect effects of glycans on antigenicity. They support the ancillary hypothesis, formulated at the beginning of this section, of indirect effects acting across the three purification-bNAb epitopes.

As described above, the sensitivity to the autologous NAbs, directed to the epitope around the V4-β19 transition, correlated inversely with PGT151 antigenicity (Fig 3B), just as PGT145 and PGT151 antigenicities were inversely related (Fig 2). Notably, the glycans most closely surrounding the V4-β19-glycan defect depended on the purification bNAb in a manner that suggests shielding of the epitope on the PGT151-purified trimer: elevated $Man_9GlcNAc_2$ on N332 and N386, whereas the shorter $Man_5GlcNAc_2$ and $Man_6GlcNAc_2$ on N339 were less abundant than on PGT145-purified trimer, which also had more $Man_5GlcNAc_2$ at N407 than 2G12-purified trimer (**Figs** 8B; **S3B**). Hence, these larger oligo-mannose-type glycans would obstruct the autologous-NAb epitope at the bottom of the V4-β19 glycan-hole more on the PGT151- than the PGT145-purified trimer.

CHO cells, although convenient for producing large enough amounts of high-quality trimer for mass spectrometry, differ subtly in glycan processing from HEK-293T cells, in which PV was produced. We therefore also expressed trimer in HEK-293F cells, which give better yields of trimer than do the HEK-293T cells from which they are derived. The glycan composition on CHO- and HEK-293F-cell-expressed trimer was compared by LC-MC. The differentially expressed forms of trimer both varied in the site-specific content of oligomannose-type glycan after the three different purifications (Fig 9). Overall, sites displaying an abundance of oligomannose-type glycans did so similarly on the trimer forms derived from the two cell lines, multiple sites containing almost 100% oligomannose-type glycans regardless of cell origin and purification method. That similarity notwithstanding, a modest tendency for higher oligomannose-type glycans on CHO- than on HEK-293F-derived trimer across the purifications occurred; at N133 on PGT151-purified trimer that difference was pronounced. That tendency was also consistent among the three purification methods at N276, where the CHO-derived trimer displayed ~70% oligomannose-type glycans and HEK-293F-derived trimer only ~50%. Conversely, we note low oligomannose content at N230, only on PGT145- and

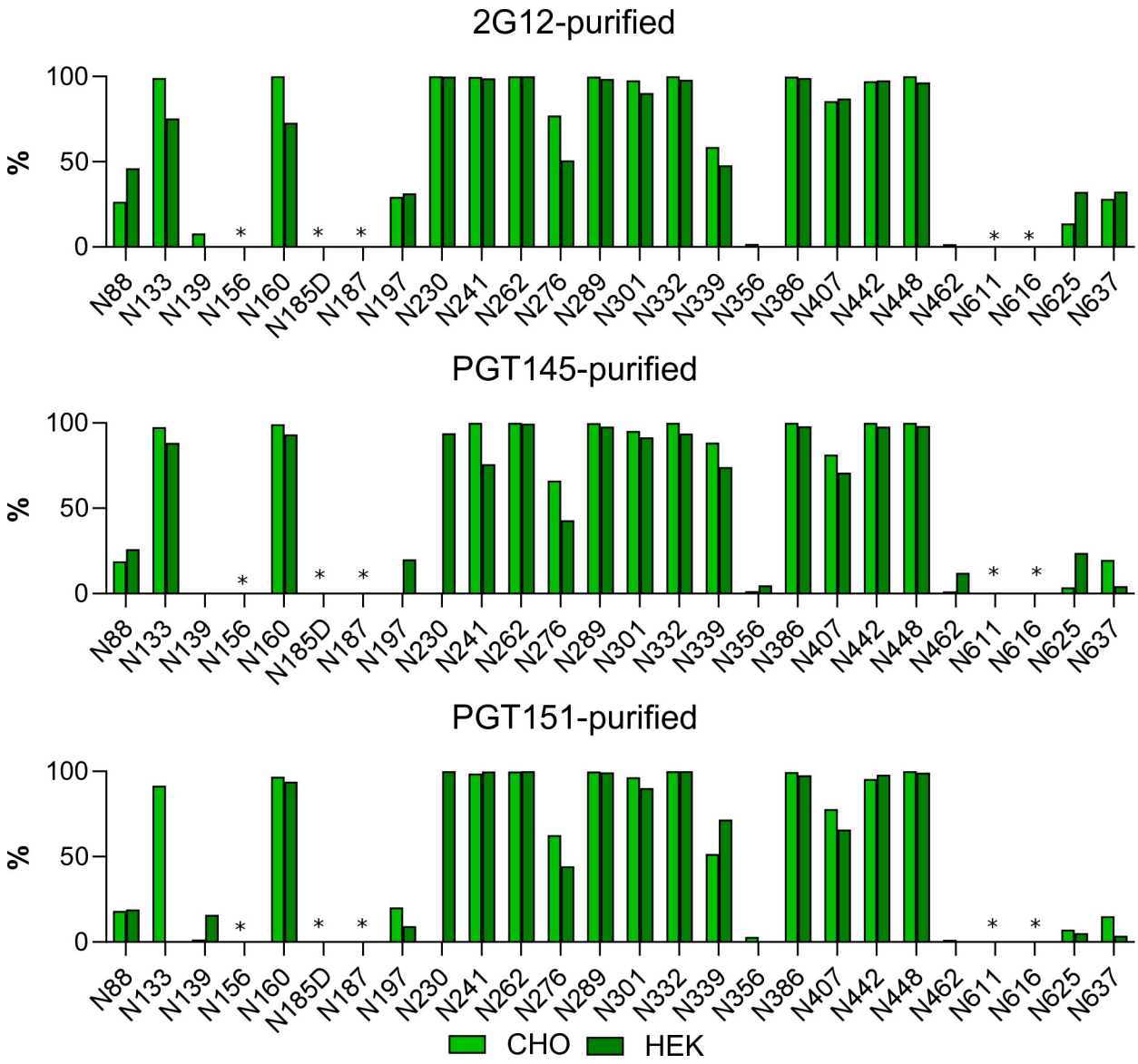

Fig 9. Comparison of CZA97.012 SOSIP.664 trimer produced in different cell lines and differentially affinity-purified. Trimer produced in either a stable CHO cell line or by transient transfection of HEK-293F cells was 2G12-, PGT145-, or PGT151-affinity- and then SEC-purified. Site-specific glycan content was determined by LC-MS on intact glycopeptides as in Fig 8B, but here the contents of oligomannose-type glycans were summed up, *i.e.*, only $Man_9GlcNAc_2$, $Man_8GlcNAc_2$, $Man_7GlcNAc_2$, $Man_6GlcNAc_2$, and $Man_5GlcNAc_2$ together, and expressed as percentages of total glycan per site. The bar charts thus represent the relative accumulated oligomannose-type glycan content at each PNGS in CZA97.012 SOSIP.664. Light green represents CHO-derived and dark green HEK-293F-derived trimer (see legend). Sites for which glycopeptides of sufficient quality could not be obtained are left non-determined and are marked with asterisks.

https://doi.org/10.1371/journal.ppat.1011601.g009

PGT151-purifed CHO-derived trimer. Overall, however, the glycosylation of trimer molecules in the two cell lines was similar.

In conclusion, varied glycosylation at sites affecting the 2G12, PGT145, and PGT151 epitopes confer differential affinity purifications by these bNAbs. That segregation is corroborated in binding analyses and explains the differential neutralization potencies and efficacies (**Figs** 2,3,5, and 6). Some glycan variations may confer antigenic heterogeneity through direct effects on paratope contacts, whereas others probably influence antigenicity indirectly. The

direct and indirect effects may interact in various combinations, together causing substantial antigenic heterogeneity.

Comparison of 3BNC117 and PGT151 neutralization with the kinetics and stoichiometry of trimer binding by their Fabs

We expanded the analyses to include neutralization by bNAb 3BNC117 and detailed binding properties of 3BNC117 and PGT151. The reason was to complement the comparator PGT145, whose interaction with CZA97.012 Env, on PV and as SOSIP trimer, has some unusual features. One is that PGT145-affinity purification of CZA97.12 SOSIP.664 yields low amounts of trimer [70]. Therefore, in a previous study, we introduced mutations into CZA97.12 SOSIP.664 to enhance the interaction, which increased affinity 14-fold. The stoichiometry, however, remained low at 0.48 [70]. Since our aim was analysis of binding relevant to neutralization, we did not use those mutations here. The moderate affinity of PGT145 Fab for CZA97.12 SOSIP.664 (K_D = 36 nM for a conformational-change model in [70]) agrees with the moderate potency of neutralization (IC_{50} 7.6 μg/ml, *i.e.*, 51 nM IgG in **Fig 1A**). The Hill coefficient of the neutralization curve, however, was low for PGT145 (h = 0.45) compared with that for PGT151 (h = 0.93, constants derived from data in **Fig 1A**). Since the stoichiometry of PGT145 binding has a maximum of one paratope per trimer, negative cooperativity cannot explain the low slope, which is therefore more plausibly due to antigenic heterogeneity among the virion Env spikes [1,48,69,98]. Hence, the Env spikes on virions might have a wide detectable-affinity spectrum covering nearly the entire population, whereas ~50% of the soluble trimer molecules are completely non-antigenic [70], a discrepancy possibly arising from differences in glycosylation between the two trimer populations [62,74,99,100]. These features combined render the PGT145-CZA97.012 interaction a complicated outlier. We therefore selected one other bNAb to compare with PGT151, *viz.* 3BNC117 [69,73]. Another reason to study neutralization and binding by 3BNC117 was that its Fab in complex with CZA97.012 SOSIP.664 yielded a high-resolution structure (see below).

The IC_{50} of the neutralization of CZA97.012 PV by 3BNC117 was 0.32 μg/ml; the maximum neutralization was close to 100%. Only in the log-log plot could a tendency towards a PF plateau above 50 μg/ml of bNAb be discerned (**Fig 10A**). Single-cycle SPR analysis showed high affinity, slow dissociation, and a high stoichiometry of 2.8, close to the ideal 3.0 for this bNAb [69]; the binding data fitted eminently well to a simple Langmuir model (**Fig 10B and S1 Table,** single-cycle kinetics; comparison with multi-cycle kinetics, **S4 Fig and S2 Table**). If 3BNC117 IgG bound with the same functional affinity as Fab to Env on PV, the IC_{50} would correspond to an average occupancy of 0.28 on its epitopes. Hence, with random distribution, 63% of the Env spikes would be occupied by at least one bNAb molecule according to the Law of Mass Action combined with binomial analysis (*cf.* [79]). These proportions of virions neutralized and of Env spikes occupied correspond to a plausible threshold of neutralization [79]. The IC_{50}(IgG)/K_D(Fab) ratio ~0.40 is compatible with a low but not necessarily negligible degree of bivalent binding. Indeed, IgG neutralizes only marginally or moderately more potently than Fab, with some variation among other HIV-1 PV-bNAb combinations; that the ratios are not higher is attributed to the low Env spike density on virions [48,90,91].

The binding of titrated PGT151 Fab was also analyzed by SPR, performed as single-cycle kinetics (**Fig 11**, **S2 Table**; comparison with multi-cycle kinetics, **S4 Fig**). Both conformational-change and heterogeneous-ligand models gave considerably better fits than a Langmuir model. To adjudicate between the former two, we performed an injection-time test. The dissociation curves after 30s and 300s association were approximately superimposable, without any tangible retardation of dissociation after the longer association. That similarity suggests an

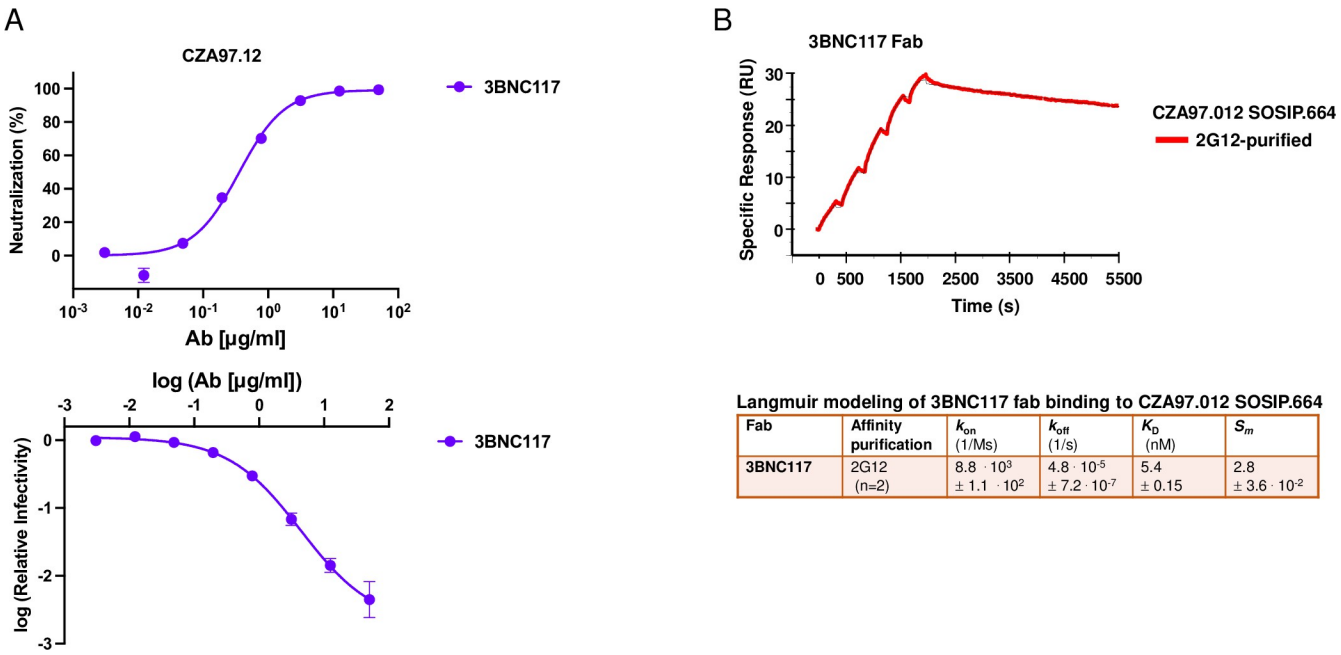

Langmuir modeling of 3BNC117 fab binding to CZA97.012 SOSIP.664

Fab	Affinity purification	k_{on} (1/Ms)	k_{off} (1/s)	K_D (nM)	S_m
3BNC117	2G12 (n=2)	$8.8 \cdot 10^3 \pm 1.1 \cdot 10^2$	$4.8 \cdot 10^{-5} \pm 7.2 \cdot 10^{-7}$	5.4 ± 0.15	$2.8 \pm 3.6 \cdot 10^{-2}$

Fig 10. Analyses of neutralization and binding by 3BNC117. A. Neutralization of CZA97.012 PV by 3BNC117 is shown. The diagram depicts a sigmoid curve fitted to % neutralization as a function of bNAb concentration (μg/ml) (top). The $\log_{10}$ of the infectivity after bNAb incubation relative to that for absence of bNAb is plotted on the y axis as a sigmoid function of the $\log_{10}$ of the bNAb concentration (μg/ml) on the x axis (bottom). The data points in both diagrams are means of two replicates ± s.e.m. **B.** SPR sensorgram for single-cycle kinetics of 3BNC117 Fab binding to 2G12- and SEC-purified CZA97.012 SOSIP.664 trimer. The sensorgram shows the cumulative binding at increasing concentrations to immobilized trimer in response units (RU), after background subtraction, on the y-axis *vs*. time (s) on the x-axis. The curve for the binding data is shown in color according to the label code; the curve for the fitted binding function is shown as a thin black line. Each association phase was 300 s; the dissociation at the end was monitored for 3600 s. The number of replicate titrations and the fitted and calculated binding parameters are given in the table underneath the sensorgram.

https://doi.org/10.1371/journal.ppat.1011601.g010

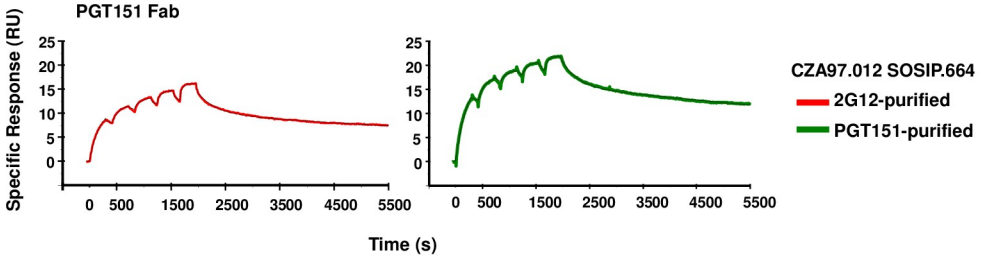

Heterogeneous-ligand modeling of PGT151 fab binding to CZA97.012 SOSIP.664

Fab	Affinity purification	k_{on1} (1/Ms)	k_{off1} (1/s)	k_{on2} (1/Ms)	k_{off2} (1/s)	K_{D1} (nM)	K_{D2} (nM)	S_{m1}	S_{m2}	$S_{m1} + S_{m2}$
PGT151	2G12 (n=2)	$7.6 \cdot 10^4 \pm 1.2 \cdot 10^3$	$8.7 \cdot 10^{-5} \pm 1.9 \cdot 10^{-6}$	$1.2 \cdot 10^4 \pm 5.3 \cdot 10^2$	$3.1 \cdot 10^{-3} \pm 1.3 \cdot 10^{-4}$	$1.1 \pm 4.2 \cdot 10^{-2}$	$2.6 \cdot 10^2 \pm 23$	$0.84 \pm 7.4 \cdot 10^{-3}$	$0.50 \pm 1.2 \cdot 10^{-2}$	$1.3 \pm 2.0 \cdot 10^{-2}$
	PGT151 (n=4)	$8.0 \cdot 10^4 \pm 4.6 \cdot 10^2$	$7.9 \cdot 10^{-5} \pm 2.2 \cdot 10^{-6}$	$1.4 \cdot 10^4 \pm 3.2 \cdot 10^2$	$3.1 \cdot 10^{-3} \pm 1.8 \cdot 10^{-4}$	$0.98 \pm 5.1 \cdot 10^{-2}$	$2.1 \cdot 10^2 \pm 12$	$1.1 \pm 1.3 \cdot 10^{-2}$	$0.48 \pm 8.4 \cdot 10^{-3}$	$1.5 \pm 2.1 \cdot 10^{-2}$

Fig 11. SPR analysis by single-cycle kinetics of PGT151 Fab binding to differentially purified CZA97.012 SOSIP.664 trimer. SPR sensorgrams for single-cycle kinetics of PGT151 Fab binding to 2G12- or PGT151- and SEC-purified CZA97.012 SOSIP.664 trimer are shown. For comparison, SPR with multi-cycle kinetics, was also performed (S4 Fig). The sensorgrams show the cumulative binding of PGT151 Fab at increasing concentrations to immobilized trimer in RU, after background subtraction, on the y-axis *vs*. time (s) on the x-axis. The curve for the binding data is shown in color according to the label code; the curve for the fitted binding function is shown as a thin black line. Each association phase was 300 s; the dissociation at the end was monitored for 3600 s. The number of replicate titrations and the fitted and calculated binding parameters are given in the table underneath the sensorgram.

https://doi.org/10.1371/journal.ppat.1011601.g011

absence of selection for or induction of a better fit [101,102]. We therefore chose the heterogeneous-ligand model (Fig 7), which was also validated by the absence of mass-transport limitation and by high T values for all four kinetic constants (S1 Table). Furthermore, the k_{on1} and k_{on2} values differed > 5.7-fold and k_{off1} and k_{off2} values > 35-fold, which means that the kinetics differ substantially between the two sites. The K_{D1} and K_{D2} values differed > 210-fold, indicating markedly distinct affinities for the two sites. The lower affinity, however, is not expected to be low enough to generate a sizeable PF, because a site with similar binding kinetics, present as a somewhat larger proportion of the total epitopes, was associated with near-complete neutralization [37].

In contrast to the kinetic constants, the stoichiometric S_{m1} and S_{m2} values differed < 2.3-fold, which means that neither subpopulation is negligible. The cumulative stoichiometry, $S_{m1} + S_{m2}$, was higher for PGT151- than 2G12-purfied trimer (1.5 ± 0.021 *vs.* 1.3 ± 0.020), which indicates that the most drastic heterogeneity in PGT151 antigenicity is reduced by the purification with the same antibody. Why it is not eliminated could have two explanations. First, the avidity difference between the polyvalency in the purification and the monovalency of Fab binding: some interactions with forms of the heterogeneous antigen may be too weak to register by SPR but could contribute to purification through crosslinking of single trimer molecules by two adjacently immobilized copies of PGT151. Secondly, a partial re-equilibration between antigenic conformers may occur after elution. Most important, however, is that for both purifications, stoichiometry of PGT151 binding was substantially lower (*viz.* 1.2 and 1.5) than its ideal value of ~2.0 measured for SOSIP trimers derived from viruses that are neutralized to near completion, such as BG505 and JR-FL [37,40,68].

Structural interpretation of the antigenic heterogeneity

To put the glycan heterogeneity and antigenicity into structural perspective, we complexed CZA97.012 SOSIP (produced in HEK-293F cells and purified by PGT151-affinity chromatography) with the Fab of the CD4-bs-specific bNAb 3BNC117 (to facilitate orientation sampling) and determined a ~3.4-Å cryo-EM structure (Fig 12A and 12B, (EMD-40088 and PDB 8gje)).

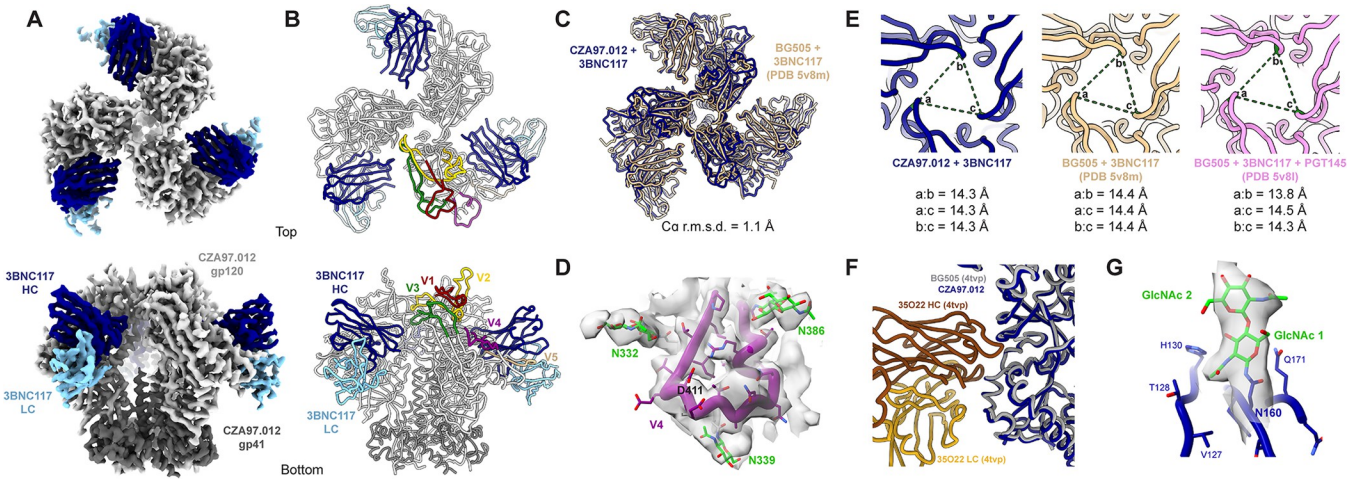

Fig 12. The CZA97.012 SOSIP.664-trimer structure. A. The 3.4-Å cryo-EM reconstruction of CZA97.012 SOSIP in complex with 3BNC117 Fab is colored as labeled. **B**. The atomic model of the CZA97.012 complex highlights gp120 variable regions. **C**. Alignment of all 6 Env chains (3-gp120, 3-gp41) of BG505 +3BNC117 (PDB 5v8m) onto the CZA97.012+3BNC117 model. Root- mean-square deviation (r.m.s.d.) was calculated between backbone Cα atoms. **D**. Map (contoured at 5σ) and model of the CZA97.012 V4-β19 region and surrounding N-linked glycans are shown. **E**. Interprotomer distances between R166 Cα in CZA97.012+3BNC117, BG505+3BNC117 (PDB 5v8m), and BG505+3BNC117+PGT145 (PDB 5v8l) are given. **F**. Alignment of BG505 SOSIP.664+35O22 (PDB 4tvp (112)) onto CZA97.012+3BNC117, with a focus on the gp41 part of the epitope. **G**. Map (contoured at 5σ) and model of the first two GlcNAc residues of at N160 and surrounding residues of one protomer of CZA97.012 SOSIP.664.

https://doi.org/10.1371/journal.ppat.1011601.g012

Overall, the Env-trimer structure resembles that of previously published ones: the Cα root-mean-square deviation (r.m.s.d.) from BG505 SOSIP.664, also in complex with only 3BNC117, is 1.1 Å (**Fig 12C**). The V4 loop, shorter than in other Env trimers that have been structurally analyzed, is fully resolved, suggesting a more stable antigenic surface, while the aforementioned region around D411 is exposed and flanked by the N332, N339, N386, and N407 glycans (**Fig 12D**). The exposure of the autologous epitope in the glycan defect around D411 explains its high immunogenicity [71]. But, in line with differential trimer purification and autologous neutralization results, it would be particularly exposed on the most PGT145-reactive Env spikes, whereas on PGT151-high-affinity trimer molecules, larger oligo-mannose-type glycans would impinge upon it (**Figs 3B, 8B,** and **S3 Fig**).

A comparison of the CZA97.012 SOSIP.664+3BNC117 structure with that of the BG505 SOSIP.664+3BNC117 complex and with that of the BG505 SOSIP.664+3BNC117+PGT145 complex (69) demonstrated that the PGT145 epitope was conformationally intact on the CZA97.012 trimer: PGT145-interacting Env residues in BG505 Env are mostly identical in CZA97.012 Env, and the opening at the apex – measured as pairwise Cα distances of R166 across protomers – is essentially the same across the 3 structures (maximum difference of 0.5 Å) (**Fig 12E**).

Still, PGT151 purification might somehow affect the dynamics of Env opening and closing through the engagement and subsequent release of the FP. The FP relocates in concert with trimer opening: in the closed state the FP is seemingly solvent-accessible and the N-terminus is disordered in most structures, being intrinsically flexible; in the open state that is induced by sCD4 engagement, the FP becomes more structured and moves towards the core of the trimer [103]. Earlier studies showed that pre-binding of sCD4 impedes PGT145 binding: the antibody cannot bind an open trimer [69]. If binding and elution from PGT151 perturbed the dynamics of the FP, so that a subset of Env molecules remained more open, then that would decrease binding of PGT145. But cryo-EM of 3BNC117 in complex with PGT151-purified CZA97.012 SOSIP.664 showed only closed trimer, demonstrating that PGT151 purification does not irreversibly open the trimer. The closed CZA97.012 trimer (in the context of bound 3BNC117) presents a similar gp41 topology to that of 35O22-bound BG505 (**Fig 12F**). Furthermore, NS-EM demonstrated that after differential-affinity and then SEC purification, CZA97.012 SOSIP.664 was all trimeric (**Fig 4B**). Hence, the observed antigenicity differences do not result from dimer or monomer contamination. Our structural analysis therefore concludes that PGT151-purified CZA97.012 SOSIP.664 resembles native-like trimer in the areas of its bNAb-epitope clusters and maintains a closed conformation.

Density for the first two GlcNAc residues of the N160 glycan is visible in the cryo-EM map, suggesting that PGT151 purification is not selecting for glycan underoccupancy at this key PGT145 site. Any such selection would have had to be allosterically mediated because of the distance from the PGT151 epitope to the trimer apex (**Fig 12G**).

Taken together, the observations of a closed conformation and of full glycan occupancy at N160 of PGT151-purified trimer suggest that differences in binding and neutralization after trimer purification or PV depletion with PGT145 and PGT151 therefore most likely stem from the other glycosylation heterogeneities at the respective epitopes that we describe above (**Figs 7–9**).

In summary, variation in the occupancy by and composition of glycans at sites affecting the 2G12, PGT145, and PGT151 epitopes is a plausible contributor to differential binding and neutralization efficacies and potencies. Some glycan variations confer antigenic heterogeneity through direct effects on paratope contacts, while others may do so allosterically.

Discussion

Clonal CZA97.012 Env trimer molecules, both on PVs and as soluble SOSIP protein, contained antigenically distinct forms of the PGT145 and PGT151 epitopes. The populations of Env-trimer molecules thus apparently have overlapping spectra of antigenicities with discrete maxima for these bNAbs. CZA97.012 Env displayed varied glycan composition at 20 PNGSs, including glycans crucially contributing to the epitopes of the affinity-purification bNAbs. Therefore, both direct and indirect effects of glycan differences on the epitopes can be deduced. Fig 13 outlines the progression from hypothesis to experiments and finally onto the wider implications for the HIV-1 bNAb field.

How can glycosylation and conformation as causes of the PF be dissected? Here, FFF-MALS demonstrated that soluble trimers affinity-purified with the different bNAbs had distinct masses and hydrodynamic radii. Whereas the radii could change along with the conformation, significant mass differences would incontrovertibly demonstrate differences in post-translational modifications, largely comprising variations in glycan-site occupancy and glycan processing [50–55,57]. The differences in mass detected by FFF-MALS among the differentially purified trimer populations were, however, merely compatible with differential processing; they were too small to prove it. But the glycan analyses were definitive on this point. Specifically, at N160, PGT145-purified trimer had less $Man_9GlcNAc_2$, $Man_8GlcNAc_2$, and $Man_7GlcNAc_2$ but more $Man_6GlcNAc_2$ than trimer purified by the other two bNAbs, and more $Man_5GlcNAc_2$ than on PGT151-purified trimer. These observations agree with structural indications of which type of glycan is best tolerated by the PGT145 paratope at that site, because cryo-EM of BG505 SOSIP.664 in complex with PGT145 Fab showed a density at N160 strongly resembling $Man_6GlcNAc_2$ [69].

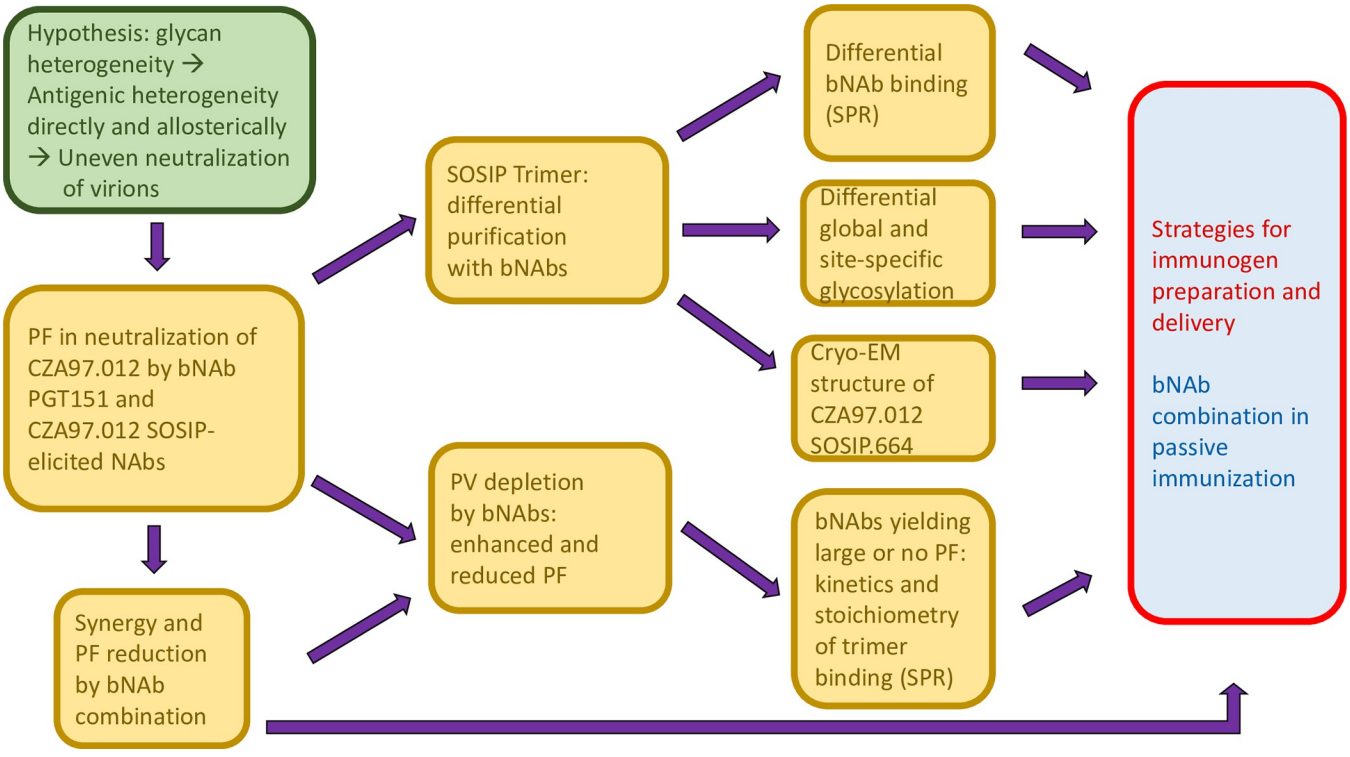

Fig 13. Flow chart from hypothesis to experiments and implications for the HIV-1 bNAb field. The main hypothesis is presented in the green shape to the left. Experimental approaches and findings are listed in golden boxes with a progression from left to right. Wider implications for the HIV-1 bNAb field, *i.e.*, active and passive immunization, are indicated in red and blue to the right.

https://doi.org/10.1371/journal.ppat.1011601.g013

Most important for explaining the large PF in PGT151 neutralization was the low stoichiometry, detected by SPR, of 1.3 PGT151 Fabs per 2G12-purified trimer (**Fig 11**). This value is substantially lower than the ideal binding of two PGT151 Fabs per trimer observed with versions of the BG505 SOSIP trimer [48,68,104]. The reduced stoichiometry could arise as an average of different proportions of occupancy by 0 or 2 Fabs or possibly by 1. Even the PGT151-purified trimer did not show the ideal stoichiometry of 2, but an intermediate one of 1.5, which suggests some trimer molecules eluted from the affinity-chromatography column could bind only 1 Fab. The corresponding proportion of un- or underoccupied Env spikes on virions could be enough to cause a sizable PF [79].

Which glycan differences within the trimer population could explain the reduced stoichiometry of PGT151 binding? A complex glycan at N611 directly interacts with the PGT151 paratope [68]. BG505, which is neutralized without any detectable PF by PGT151 [37], has exclusively complex glycans at N611 both on membrane-anchored Env spikes and SOSIP.664 trimer [62,68]. Notably, the CZA97.012 SOSIP.664 trimer had equal proportions of oligomannose- or hybrid-type and complex glycan at N611 after the non-segregating purification by 2G12, a majority of oligomannose- or hybrid-type glycan after PGT145 purification, and exclusively complex glycan after PGT151 purification (**Fig 7**). The oligomannose- or hybrid-type glycan at N611 in the mixed trimer population quite plausibly reduces the average stoichiometry of PGT151 Fab binding (**Fig 11**), and thereby causes the large PF (**Fig 1**). Full N611 occupancy by particular complex glycans would be conducive to the ideal stoichiometry of two paratopes per trimer (**Fig 7**). Additionally, the observed heterogeneity in the precise type of complex glycan at N637 among the antigenic forms purified by the respective bNAbs, perhaps in combination with allosteric glycan effects, could modulate stoichiometry and thereby neutralization efficacy (**Fig 8**).

A potential caveat in these dissections of PF causality is that differences in glycosylation between certain sites on soluble and viral-membrane-anchored trimer molecules have been observed for some strains [62,99]. But those are not uniform occurrences. Much evidence supports eminent similarity in antigenicity and glycosylation patterns between membrane anchored Env spikes on virions and several SOSIP trimers studied [48,49,62,85,87,99,103,105–113]. Overall, the following explanatory scenario therefore seems justified. A primordial heterogeneity in glycosylation arises in the endoplasmic reticulum as varied occupancy and in the Golgi as varied type of glycan. This variation would then manifest itself in antigenic heterogeneity through direct paratope contact effects and allosteric effects on glycan and amino-acid side-chain orientation, as well as on backbone conformation. Such combined net effects would increase or decrease the stoichiometry of binding. Ultimately, as a result, the stoichiometry falls above or below a minimum threshold of paratopes bound per virion required for neutralization [1,7,24,79,84,114–116].

It may be fruitful to compare how the PF is caused in PGT151 neutralization of B41 [37] and of CZA97.012. Structural studies could attribute the large B41 PF to the pronounced conformational flexibility of the B41 trimer [87,103,117], specifically to the opening of the trimer yielding either steric clashes with the PGT151 paratope or the sequestering of a key component of the epitope, *viz*. the FP [37]. Although the trimer opening would be a sufficient cause of the large PF, the propensity for a sub-population of trimer molecules to assume or stay in an open conformation can have a number of antecedent causes, including allosteric effects of heterogeneous glycosylation [37]. But B41 may be a special case: the conformational flexibility of its Env protein is unusual among the different HIV-1-derived trimers studied so far [103,117]. Large PFs in PGT151 neutralization, in contrast, are common [37,40]. Thus, the intriguing explanation for the large PF in PGT151 neutralization of B41 [37] lacks the requisite generality to explain a fairly frequent phenomenon. Here we present a hypothesis about PGT151

neutralization that does not: our findings support direct and indirect effects of widespread heterogeneity in glycosylation, which stems from the high glycan density on Env and myriad stochastic fates along the secretory pathway. The hypotheses imply discrepancies in global glycan composition, heterogeneity in paratope-contacting glycans, and multiple glycan differences with potential allosteric effects. On all counts we found evidence for such variation, which would give antigenic heterogeneity and thereby PF variations (**Figs** 7 and 8).

How do the findings about the PF and glycosylation inform immunogen design? Just as for B41, which also shows a large PF in PGT151 neutralization [37], the PGT145 and PGT151 epitopes on the CZA97.012 trimer seem allosterically interconnected. In the case of both virus isolates, their antigenic maxima are discrete in the trimer population, and antigenic variants with lower PGT151 affinity present the main autologous epitope in a more accessible or paratope-fitting form than do the average trimer molecules (**Fig 3**, [37]). But the epitopes for autologous neutralization are located in distinct regions on the B41 and on CZA97.012 trimers. Both of them, however, line defects in the glycan shield: on the B41 trimer around residues 230 and 289 and on the CZA97.012 trimer around residue D411 at the V4-β19 transition [71,118,119].

The inverse relationship between PGT151 binding and autologous neutralization was here further corroborated by association between the magnitude of the effect of PV depletion by PGT151 and of the D411N-KI mutation on the neutralizing capacities of the autologous rabbit sera (**Figs** 3 and **S3**). The interconnectedness of the bNAb and autologous epitopes might suggest allosteric effects of plugging the glycan defect, but we found no evidence for that: the bNAbs tested neutralized the KI mutant and the parental virus similarly (**S2 Fig**). Nevertheless, if preferential presentations of the autologous and the PGT151 epitopes by isoforms are incompatible, which form would best induce breadth? Efforts to broaden autologous neutralization responses to partly overlapping glycan-defect epitopes on B41 and BG505 Env seem to abut intricate molecular barriers [119]. If those responses are not amenable to broadening, they must be considered off-target [120]. Do the responses to the glycan-defect epitope centered on D411 on CZA97.012 Env hold any greater prospect for broadening?

The high-resolution structure of the previously uncharacterized CZA97.012 SOSIP.664 trimer we present here may help answer that question (**Fig 12**). In contrast to other structurally analyzed Env trimers, the CZA97.012 trimer has a fully resolved V4 loop, which suggests a relatively stable antigenic surface there, probably because the shortness of this loop, a characteristic of Clade C isolates [121]. This greater stability might favor certain broad but clade-restricted NAb responses [122–125]. Whether this stability and exposure are conducive to eliciting intra-Clade breadth or merely promote off-target narrow responses cannot de determined by our data. But the structural information may assist the design of mutants that promote intra-clade-broadening of autologous responses, without compromising the structural integrity of known cross-clade bNAb epitopes (cf. [119]).

Since preferential PGT151 binding and neutralization were linked to similarly superior activities of other FP-directed bNAbs (**Figs** 3, 5, and 6), PGT151-purifed immunogens might generally favor the induction of such bNAbs. Furthermore, PGT151-affinity purification reduced PGT145 binding less than *vice versa*, whereas only PGT145-affinity purification reduced PGT121 and VRC01 binding. In accordance with these effects, PGT151-purified immunogens might induce more advantageous responses. Still, PGT145 purification enhanced and PGT151 reduced 3BC315 binding to its inter-protomeric gp41epitope. Thus, mixtures of differentially purified immunogens might be optimal, since bNAbs of many specificities are desirable, for reasons we conclude with below. Or alternatively, immunogens purified with, *e.g.*, 2G12 and SEC [126], which segregates antigenic forms less than do PGT145 and PGT151, might elicit multiple bNAb specificities. Such strategies might achieve the ideal of heterogeneous immunogen preparations comprising multiple glycoforms (**Fig 13**).

Now, mRNA delivery, which is successful in SARS-CoV-2 vaccination [127,128], may also be harnessed for HIV-1-vaccine development. The Env expressed *in vivo* after mRNA inoculation will differ somewhat in glycan composition from Env expressed *in vitro* in immunogen-production cells, particularly when those are derived from other species [129]. But the drawbacks and benefits of those differences fall beyond our current scope: the question here is how heterogeneous are the glycans that mRNA-expressed Env harbors. Some heterogeneity will inevitably arise through stochastic events along the secretory pathway. Arguably, the diversity of glycoforms on the surface of individual transduced cells, and *a fortiori* on the surface of cells of different types (cf. [130,131]), would be greater than in Env purified with single, highly glycoform-selective bNAbs. Ultimately though, this issue must be settled by glycan analyses, such as those described in this study, of mRNA-expressed Env.

Large PFs *in vivo* would be problematic after both the successful induction of bNAbs by active immunization and the administration of bNAbs as passive immunization for prevention or therapy [10,12,132] (**Fig 13**). Several factors may conspire to reduce both efficacy and potency *in vivo* compared with *in vitro*: PV is more sensitive to neutralization than fully replicating virus, and virus derived from transfected 293T cells is more sensitive than that derived from primary lymphocytes, which is in turn more sensitive than virus produced in macrophages [130,131,133], the latter difference having been attributed to N-linked lactoseaminoglycans, present exclusively on macrophage-derived Env [131]. As yet another factor differentiating neutralization *in vivo* from that *in vitro*, HIV-1 is more genetically diverse *in vivo* than *in vitro*, which raises the bar for entry inhibition [29]. The resulting size of the PF *in vivo* after exposure of vaccinees or recipients of bNAbs for prevention could make the difference between sterilizing immunity and established infection [17,37,132].

The PF in therapeutic passive immunization could undermine the therapeutic suppression of viremia and curative attempts to eliminate recalcitrant viral reservoirs. The PF might be caused by post-translationally determined glycan heterogeneity, because the outgrowth virus isolated from the HIV-1 reservoir after bNAb therapy is often largely sensitive to the treatment bNAbs [134–136]. Therefore, sizeable PFs in neutralization by the treatment bNAbs could be due to epigenetic resistance that creates and maintains the reservoir.

Our findings of PF reduction, as well as of substantial synergy in potency at 80% inhibition, by a combination of bNAbs support the advantage of multiple bNAb specificities both in active and passive immunization [137–141] (**Fig 13**). The explanation for this enhanced neutralization would be differential antigenicities, partly segregated over the virion population [1,29,79]. Such a complementarity-based explanation can even account for enhanced neutralization between NAbs directed to the same epitope cluster, provided the trimer population on virions presents antigenic variants that interact differentially with those NAbs [142].

To conclude, the PF in HIV-1 neutralization can be explained by antigenic heterogeneity that reduces stoichiometry of NAb binding through multiple post-translational modifications, in particular heterogeneous glycosylation, which acts directly or allosterically, alone or in unison with conformational variability; the PF can be minimized by combining multiple bNAb specificities.

Materials and methods

PV production

HEK-293T cells, maintained in growth medium (DMEM with 10% FBS, 2mM L-Glutamine, and 1% penicillin-streptomycin), were used for producing PV. One day before transfection, cells were seeded in 6-welled plates at a density of 4×10^5 cells/well. Transient transfection was performed with ProFection Mammalian Transfection System (Promega), which is calcium-

phosphate-based, in accordance with the manufacturer's protocol. Three hours before transfection, the medium of 50–60%-confluent cell cultures was changed to antibiotic-free. Cells were transfected with CZA97.012 *env* pcDNA3 and pNL4.1AM *env* (-) *luc* (+) plasmids (ratio of 1:2) diluted in $CaCl_2$ (2M) and mixed with transfection reagent in 2 × saline solution buffered with 4-(2-hydroxyethyl)-1-piperazineethanesulfonic acid-buffered (HEPES). The transfection mix was added to the cells and incubated at 37˚C in air containing 5% CO_2. The next day, cells were supplemented with fresh growth medium and incubated further for 48h. PV was harvested 72 h post-transfection by spinning the supernatant at 2000 rpm for 10 min. An additional 10% FBS was added to the supernatant, before spinning, to maintain virion integrity.

TZM-bl neutralization assay

Neutralization of PV by bNAbs and heat-inactivated sera was analyzed in a TZM-bl-cell-based assay, as described [143]. The day before infection, cells were seeded in 96-well plate (white tissue-culture treated, Costar 3917), at a density of 1×10^4 cells per well. PV (diluted in DMEM growth medium to yield luminosity readouts of ~2000 000 counts/s) were incubated with serially diluted bNAbs or sera (heat-inactivated) for 1 h at 37˚C. The high dose was chosen to obtain a wide dynamic range, which allows sensitive PF identification. We verified complete absence of bleed-through of signal to neighboring wells, even at this high viral dose. The mixtures of PV and bNAb or serum were transferred to TZM-bl-cell cultures. Three days after infection, medium was aspirated and the cells were lysed with Glo-lysis buffer (Promega). Plates were frozen for at least 2 h at -80˚C. After thawing, Bright-Glo substrate was added to each well. The luciferase signal was read on an Enspire multimode plate reader (Perkin Elmer). Relative infectivity was analyzed by subtracting the background signals (cells but no virus) from signals of virus-cell wells. The neutralization (%) in relation to the infectivity of virus without Ab was calculated for all bNAb and serum dilutions. The signal in the absence of antibody was stipulated to represent 100% infectivity, *i.e*., 0% neutralization. Data were analyzed and plotted with Graph Pad Prism 6 software; four-parameter sigmoid curves were fitted to the data with maximum constrained to 100%. The assay described above was used to generate the results in **Figs 1–3**, **10**, and **S2-S3.** In **S1 Fig** a variant of the assay was used, with a constant bNAb concentration (50 μg/ml) and a titrated viral input. The D411N mutant **(S2 and S3 Figs)** has been described previously in a study mapping of autologous neutralizing responses of rabbits to CZA97.012 SOSIP.664 immunization [71].

Depletion of PV by bNAbs

PV was added to affinity columns containing Sepharose beads with covalently coupled PGT145 or PGT151 or without Ab (mock control). The bNAb affinity columns were made by cross-linking IgG to activated CNBr-Sepharose 4B beads (GE Healthcare) according to the manufacturer's instructions and as previously described [87]. The columns containing PV and beads were incubated at 37˚C for 3 h with constant mixing on a nutator. Initially, to assess the effect of temperature and nutation, aliquots of PV without beads, designated un-depleted PV, were subjected to the same treatment. Un-depleted and mock-depleted PV later showed indistinguishable neutralization, and the un-depleted control was discontinued. The mix of PV plus beads was allowed to settle at room temperature in vertical columns. PV was collected by gravity flow-through from the respective column, filtered through 0.45-μm membranes, and immediately analyzed in a neutralization assay.

Expression and selective purification of native Env trimer

First, trimer was produced and differentially purified from a CZA97.012 SOSIP.664-expressing CHO-cell line maintained in ExpiCHO Expression Medium (Thermo Fisher Scientific) [70]. Then, the CZA97.012 SOSIP.664 trimer was also expressed transiently in HEK-293F where indicated. Cells were cultured in Expi293 Expression Medium (Thermo Fisher Scientific) supplemented with 1 × penicillin-streptomycin. The construct CZA97.012 SOSIP.664 with His-tag (GSGSGGSGHHHHHHHH) was cloned into the pPPI4 expression vector (GenScript). HEK-293F cells were transiently transfected by the use of 293fectin (Thermo Fisher Scientific). Briefly, cells were seeded at a density of 4×10^6 cells/ml in 250 ml of medium (with antibiotics), a day before transfection. On the day of transfection, cells were suspended in antibiotic-free medium at 6.0×10^6 cells/ml with 90% viability as measured by trypan blue exclusion. *CZA97.012 SOSIP.664* and *furin* plasmids were diluted in Opti-MEM at a ratio of 4:1, mixed with 293fectin reagent, and incubated at room temperature for 20 min. The 293fectin-DNA mix was added to the cells. Transfected cells were incubated at 37˚C with 5% CO_2 and constant shaking for 3 days. Then cells were centrifuged at 3000 rpm for 30 min. Supernatant was collected, passed through a 0.2-μm filter in preparation for 2G12-, PGT145-, and PGT151-affinity purification. bNAb affinity columns were made by cross-linking IgG to activated CNBr-Sepharose 4B beads (GE Healthcare) according to the manufacturer's instructions. The filtered supernatant was allowed to pass through the affinity columns. Bound trimer was eluted with 3M $MgCl_2$, as described elsewhere [70]. $MgCl_2$ was removed by dialyzing through snake-skin tubing in an exchange buffer (TN150: 20mM Tris-HCl, 150mM NaCl, pH 8) overnight at 4˚C. SEC with TN150 as running buffer was then performed on a Hi Load 16/600 Superdex 250 pg column, to remove aggregates, dimers, and monomers. The fractions were assessed on Blue Native-PAGE; pure-trimer fractions were pooled and stored at -80˚C till further analysis. Protein concentration was determined by the bicinchoninic assay (BCA). PGT145-purification yields were 10–20% and PGT151-purification yields were 20–30% of the yield of Env obtained with 2G12 purification. Subsequent SEC yields were 30–40% trimer from 2G12-, 50–100% from PGT145-, and 70–100% from PGT151-purified Env.

Field-flow fractionation (FFF) and multi-angle light scattering (MALS)

FFF experiments were performed with an Eclipse DualTec module (Wyatt Technology Corporation) running on an Agilent 1260 Infinity II platform (Agilent Technologies). Each sample (50 μg) was loaded onto a short channel unit assembled with a wide 350-μm spacer and a regenerated cellulose membrane (molecular-mass cutoff = 10 kDa). The detector flow was set to 0.4 ml/min, while cross-flow was 0.8 ml/min in all measurements. Total run length was 100 min. The FFF system is coupled with an in-line MiniDawn Treos multiangle light scattering (MALS) detector, a quasi-elastic light scattering (QELS) detector, and an Optilab T-reX refractive index (RI) detector (Wyatt Technology Corporation). Molar mass and hydration radius (R_h) values for different samples were determined based on the analysis of the light scattering and absorbance at UV 280 nm in Astra V software. These values were calculated only for the trimer-corresponding peak. Appropriate UV-280-nm extinction coefficients were applied for each sample. Refractive index increment (dn/dc) was set to 0.168, a value experimentally determined for fully glycosylated Env [144].

Negative-stain electron microscopy (NS-EM)

Samples were diluted to ~0.02 mg/mL final trimer concentration, and a 3-μl drop was applied to carbon-coated and plasma-cleaned copper mesh EM grids. The grids were stained with 2% (w/v) uranyl formate. Data were collected with an FEI Tecnai Spirit electron microscopy

operating at 120 keV and equipped with a TVIPS TemCam F416 camera. Data processing steps, including particle picking, particle extraction, and 2D classification were performed with the Appion software suite [145]. 2D class averages were analyzed and particles belonging to classes that did not unambiguously resemble native-like trimers (compact, trimeric structures) were categorized as"non-native."

Cryo-electron microscopy (cryo-EM)

A mass of 0.2 mg of CZA97.012 SOSIP trimer (expressed in HEK-293F cells and purified by PGT151-affinity chromatography) was incubated with 0.3 mg of 3BNC117 Fab overnight at room temperature (approximately 2-fold molar excess of Fab per binding site calculated from the respective peptidic molecular masses of 215 and 50 kDa). On the following day the complex was purified on a gel-filtration column (HiLoad 16/600 Superdex 200 pg (Cytiva)), and the corresponding trimer:Fab complex peak was concentrated to ~1 mg/ml. Immediately before freezing, Amphipol A8-35 (Anatrace) was added to a final concentration of 0.01% w/v to assist with particle tumbling. A 3-μl drop of the mixture was applied to a plasma-cleaned C-flat 2/2 holey carbon grid (Electron Microscopy Sciences), manually blotted and vitrified in liquid ethane with a homemade plunger.

Data were collected on a Thermo Fisher Titan Krios (300 keV) and a Gatan K2 Summit (4K × 4K) camera with Leginon software [146]. The nominal magnification was 22500-fold resulting in a pixel size of 1.31 Å. A total of 1142 micrographs were collected in a defocus range of -1.0 to -2.7 μm and an average dose of 58 e-/Å^2 per micrograph. Movies were aligned and dose-weighted with MotionCor2 [147] and imported into cryoSPARC [148]. CTF corrections were performed with Gctf [149]. Particles were picked with a combination of Blob Picker and Template Picker and subjected to rounds of 2D classification, Ab Initio 3D modeling, Heterogenous Refinement, and Non-Uniform Refinement (with global CTF corrections). C3 symmetry was applied to the final refinement of 79 261 particle images, resulting in an estimated ~3.4-Å global FSC(0.143) resolution (**S3 Table**, **S5 Fig**).

Model building was initiated by generating a homology model of CZA97.012 with BG505 (PDB 4tvp) as the template and the UCSF Chimera [150] implementation of Modeller. Published 3BNC117 Fab models (PDB 4jpv) were fitted into the cryo-EM map. The complete model was then refined iteratively with Coot [151], Phenix real space refine [152], and Rosetta Relax [153]. Final validation was performed with the MolProbity [154] and EMRinger [155] implementations in Phenix, and statistics are summarized in **S3 Table**. The map and model have been deposited to the Electron Microscopy Data Bank and Protein Data Bank with the respective accession codes EMD-40088 and PDB 8gje.

bNAb binding analyzed by ELISA

The binding of bNAbs to distinct clusters of epitopes on the CZA97.012 SOSIP.664 trimer expressed in HEK-293F was analyzed after 2G12, PGT145, or PGT151 purification followed by SEC was analyzed by ELISA as previously described [71,87,156]. Briefly, 100 μl His-tagged trimer diluted to 1.5 μg/ml in PBS (pH 7.4) or PBS only as a control was added per well to Ni-NTA 96-well plates (Qiagen) and incubated over night at 4˚C. After three washes with TBS, wells were blocked for 30 min at room temperature with 5% Milk (Bio-Rad 1706404) in PBS (100 μl/well) and again washed three times in PBS. The bNAbs were diluted in PBS with 5% Milk and 100 μl added per well. The plates were incubated for 2h at room temperature and then washed 3 times in TBS. Secondary HRP-conjugated antibody diluted 1/3000 in PBS with 10% Milk, 100 μl per well, was added. The plates were incubated for 45 min at room temperature and washed 5 times with PBS plus 0.05% Tween. Then, 50 μl of TMB-substrate solution

was added and the plates were incubated at room temperature for 3 minutes. To terminate the reaction, 50 μl of stop solution (0.3 N H_2SO_4) was added and the absorbance read at 450 nm on an Enspire multimode plate reader (Perkin Elmer). Background signals from control wells incubated with bNAbs and then conjugate were subtracted. Sigmoid functions were fitted to the data and curves plotted in Prism (GraphPad).

Preparation of Fabs

3BNC117 and PGT151 Fabs were expressed by transient transfection of HEK-293F suspension cells with the respective *Fab* plasmids [37,104]. Fabs were affinity-purified on an anti-human-kappa-XL column, then subjected to ion-exchange fast protein liquid chromatography (ÄKTA FPLC, GE), and finally SEC. Fab purity was confirmed by reducing and non-reducing SDS-PAGE electrophoresis.

bNAb binding analyzed by SPR

Antigenicity of bNAb epitopes on the His-tagged CZA97.012 SOSIP.664 trimer expressed in HEK-293F cells and 2G12-, PGT145-, or PGT151- and then SEC-purified was also analyzed by SPR. Analyses were performed on BIAcore 3000 and T200 (Cytiva) instruments at 25˚C as previously described [48,104]. Briefly, anti-His Ab covalently coupled to a CM5 sensor chip was used for capturing the His-tagged trimer to a density (R_L value) of ~250 RU. In each cycle, fresh trimer protein was captured, and at the end of each cycle the anti-His chip was regenerated with a single pulse of 10mM glycine (pH 2.0) for 1 min. The bNAb IgG was injected at a concentration of 500 nM; association was monitored for 300 s and dissociation for 600 s. Mass transfer limitation was avoided by a high flow rate (50 μl/min), which was used throughout also for regeneration to achieve better flushing. Sensorgrams were prepared in the BIAevaluation software.

Single-cycle kinetics (SCK on the T200 instrument only) was applied to the deep analysis of the binding of Fabs of PGT151 and 3BNC117 to differentially purified His-tagged CZA97.012 SOSIP.664 trimer. In each SCK experiment, increasing concentrations of Fabs (2-fold dilution starting from 1 μM) were injected sequentially in a single cycle. Fab at each concentration was allowed to bind for 300 s to anti-His-captured trimer on the sensor surface of CM5 chips. After the final injection, the dissociation was monitored for 3600 s. At the end of the cycle, the sensor surface was regenerated as above. In each SCK assay, 2 start-up cycles and 3 zero-analyte cycles with running buffer were included.

To consolidate the SCK results, the same Fabs were also analyzed by multi-cycle kinetics (MCK also on the T200 instrument). Fab solutions were titrated in 2-fold steps from 1 μM until no signal could be detected. Fab at each concentration was injected over freshly captured trimer; association was monitored for 300 s, and dissociation for 600 s. At the end of each dissociation phase, the sensor surfaces were regenerated, as above.

Trimer immobilization for the kinetic analyses was adjusted to give $R_{max} < 30$ RU; experimental R_{max} was ~25 RU). A high flow rate (50 μl min^{-1}) was used as a further measure to prevent mass transfer limitation. SCK and MCK data were analyzed with the BIAevaluation software v3.2.1 (Cytiva). Control-channel- and zero-analyte-subtracted sensorgrams were prepared. A Langmuir model was first fitted to the kinetic data. The Langmuir fit was considered acceptable based on goodness of fit ($\chi^2<1$), significance of kinetic rate constants (T>10), uniqueness (U<15, SCK only), and the scalar values of residuals (<2 RU). For PGT151 Fab, the Langmuir fit was unsatisfactory, and conformational-change and heterogeneous-ligand models were also fitted. They fulfilled the same criteria as the Langmuir model except that they do not include uniqueness evaluation. The conformational-change modeling was further

investigated by injection-time variation: no deceleration in dissociation during 600 s was observed by reducing the association phase from 300 s to 30 s. The conformational-change modeling could therefore not be justified. Hence, the heterogeneous-ligand model was chosen and further validated (see Results). In all modeling, mass-transport limitation, counteracted by maximum flow rate and low trimer immobilization, was excluded by fulfillment of the following criteria: the mass-transfer constant, k_t, was $>10^8$ ($RU \cdot M^{-1} \cdot s^{-1}$) and its T value <10. As seen in S1 and S2 Tables, these criteria were met with margins of several orders of magnitude.

Global glycan analysis by HILIC-UPLC

The abundance of total N-linked glycans was determined after PNGase F treatment. PNGase F-released glycans were analyzed on a Waters Acquity H-Class UPLC instrument with a Glycan BEH Amide column (2.1 mm x 100 mm, 1.7 μm; Waters) and the following gradient: time (t) = 0: 22% A, 78% B (flow rate = 0.5 ml/min); t = 38.5: 44.1% A, 55.9% B (0.5 ml/min); t = 39.5: 100% A, 0% B (0.25 ml/min); t = 44.5: 100% A, 0% B (0.25 ml/min); t = 46.5: 22% A, 78% B (0.5 ml/min), where solvent A was 50 mM ammonium formate, pH 4.4 (Ludger) and B was acetonitrile. Fluorescence was measured at an excitation wavelength of 310 nm and an emission wavelength of 370 nm for procainamide, or 250 nm and 428 nm for 2-aminobenzoic acid (2-AA). Data were processed with Empower 3 software (Waters). The relative abundance of each oligomannose-type glycan released by endoglycosidase H (Endo H), *i.e.*, $Man_9GlcNAc_2$, $Man_8GlcNAc_2$, $Man_7GlcNAc_2$, $Man_6GlcNAc_2$, and $Man_5GlcNAc_2$, was calculated by comparing with the total glycan pool released by PNGase F. An aliquot of 15 μl containing trimer with fluorescently labelled glycans was treated with Endo H overnight at 37˚C (New England Biolabs). Glycans were extracted with a polyvinylidene-fluoride protein-binding membrane (Merck Millipore). Digested glycans were analyzed by HILIC-UPLC as before [52,53]. Glycans were quantified by integrating the peaks before and after glycosidase digestion, after normalization of the chromatograms.

Site-specific glycopeptide analysis by LC-MS

The analyses were performed similarly to what has been described [97]. Specifically, ~50 μg of CZA97.012 SOSIP.664 trimer was denatured, reduced, and alkylated by sequential 1-hour incubations at room temperature as follows: 50 mM Tris-HCl buffer, pH 8.0, containing 6 M urea and 5 mM DTT, then in the dark after the addition of 20 mM iodoacetamide (IAA), and finally with an increased DTT concentration (20 mM) to eliminate residual IAA. The alkylated trimer was buffer-exchanged into 50 mM Tris-HCl, pH 8.0, in Vivaspin columns and aliquoted. Protein was digested with either trypsin or chymotrypsin (Mass Spectrometry Grade, Promega) at a mass ratio of 1:30 overnight at 37˚C. Reaction mixtures were dried and glycopeptides were extracted with C18 ZipTip (Merck Millipore), following the manufacturer's protocol.

Eluted glycopeptides were dried and re-suspended in 0.1% formic acid prior to mass spectrometric analysis. Aliquots of intact glycopeptides were analyzed by nano liquid- chromatography-electrospray-ionization mass spectrometry (LC-ESI MS) with an Easy-nLC 1200 system coupled to an Orbitrap Fusion mass spectrometer (Thermo Fisher Scientific) and fragmentation by higher-energy collisional dissociation (HCD). Peptides were separated on an EasySpray PepMap RSLC C18 column (75 μm x 75 cm) with a linear gradient consisting of 0%– 32% acetonitrile in 0.1% formic acid over 240 min followed by 35 min of 80% acetonitrile in 0.1% formic acid. The flow rate was set to 300 nl/min, the spray voltage to 2.5 kV, the temperature of the heated capillary to 275˚C, and HCD energy to 50%, appropriate for the fragmentation of glycopeptide ions. Data analysis and glycopeptide identification were performed with Byonic

(Version 2.7) and Byologic software (Version 2.3; Protein Metrics Inc.), as follows. First, the mass spectrometry data and protein sequence were processed with Byonic allowing for a precursor mass tolerance of 4 ppm and a fragment mass tolerance of 10 ppm. Cleavage sites were specified as the C-terminus of Arg and Lys residues for tryptic digests, and the C-terminus of Tyr, Trp, and Phe residues for chymotryptic digests. The glycopeptide fragmentation data were then evaluated manually for each identified glycopeptide with Byologic. The peptide was validated as true-positive when the correct b and y fragment ions were observed along with oxonium ions corresponding to the identified glycan structure. The intensities of the extracted ion chromatograms (XIC) over all charge states for each true-positive glycopeptide (with the same amino-acid sequence) were calculated as percentages, to determine the relative amounts of each glycoform.

To determine the class of glycan occupying particular sites, glycopeptides were digested with Endo H, which cleaves oligomannose- and hybrid-type glycans, leaving a single GlcNAc residue at the corresponding site. The reaction mixture was then dried completely and resuspended in a mixture containing 50 mM ammonium bicarbonate and PNGase F in pure O^{18}-**labelled water** (Sigma-Aldrich) throughout. This second reaction cleaves the remaining complex-type glycans, leaving the GlcNAc residues intact. The use of H_2O^{18} in this reaction enables complex glycan sites to be differentiated from unoccupied glycan sites as the hydrolysis of the glycosidic bond by PNGase F leaves an O^{18} isotope on the aspartate residue that results from the deamidation of the asparagine. The ensuing peptides were purified by C18 ZipTip, as outlined above and subjected to LC-ESI MS as described above but with a lower HCD energy of 27%, because glycan fragmentation was not required.

Supporting information

S1 Table. Single-cycle kinetics (SCK).
(PDF)

S2 Table. Multi-cycle Kinetics (MCK).
(PDF)

S3 Table. Cryo-EM data collection, processing, and validation.
(PDF)

S1 Fig. The residual infectivity in neutralization of PV at varied dose.
(PDF)

S2 Fig. Neutralization of CZA97.012 parental and D411N-mutant PV.
(PDF)

S3 Fig. The mapping of autologous NAb epitopes in sera from rabbits immunized with CZA97.012 SOSIP.664.
(PDF)

S4 Fig. PGT151 and 3BNC117 Fab binding to CZA97.012 SOSIP.664 analyzed with multi-cycle kinetics (MCK) by SPR.
(PDF)

S5 Fig. Cryo-EM data processing.
(PDF)

Acknowledgments

The human bNAbs VRC01, 2G12, PGT121, and PGT145 [69,93,157,158] were graciously provided by the International AIDS Vaccine Initiative (IAVI, La Jolla), VRC34.01 [86] by John Mascola (VRC, NIH), 35O22 [159] by Mark Connors (VRC, NIH), and ASC202 by Marit J van Gils (AMC). Human Immunodeficiency Virus Type 1 (HIV-1) SG3ΔEnv Non-infectious Molecular Clone, ARP-11051, contributed by Drs. John C. Kappes and Xiaoyun Wu (University of Alabama Birmingham [143]), was obtained through the NIH HIV Reagent Program, Division of AIDS, NIAID. We are grateful to Erik Francomano and Oscar Feliciano for expert technical assistance.

Author Contributions

Conceptualization: Rajesh P. Ringe, P. J. Klasse.

Data curation: Rajesh P. Ringe, Philippe Colin, Gabriel Ozorowski, Anila Yasmeen, Thomas Ketas, Andrew B. Ward, Max Crispin, P. J. Klasse.

Formal analysis: Gabriel Ozorowski, Anila Yasmeen, Max Crispin, P. J. Klasse.

Funding acquisition: John P. Moore, Andrew B. Ward, Max Crispin, P. J. Klasse.

Investigation: Rajesh P. Ringe, Philippe Colin, Gabriel Ozorowski, Joel D. Allen, Anila Yasmeen, Gemma E. Seabright, Jeong Hyun Lee, Aleksandar Antanasijevic, Kimmo Rantalainen, Thomas Ketas, Andrew B. Ward, Max Crispin, P. J. Klasse.

Methodology: Rajesh P. Ringe, Philippe Colin, Gabriel Ozorowski, Joel D. Allen, Anila Yasmeen, Aleksandar Antanasijevic, Andrew B. Ward, Max Crispin, P. J. Klasse.

Project administration: P. J. Klasse.

Supervision: Thomas Ketas, Andrew B. Ward, Max Crispin, P. J. Klasse.

Validation: Thomas Ketas, Max Crispin, P. J. Klasse.

Writing – original draft: P. J. Klasse.

Writing – review & editing: Rajesh P. Ringe, Philippe Colin, Gabriel Ozorowski, Joel D. Allen, Anila Yasmeen, Gemma E. Seabright, Aleksandar Antanasijevic, John P. Moore, Andrew B. Ward, Max Crispin, P. J. Klasse.

References

1. Klasse PJ. Neutralization of Virus Infectivity by Antibodies: Old Problems in New Perspectives. Adv Biol. 2014;2014. https://doi.org/10.1155/2014/157895 PMID: 27099867
2. Cromer D, Steain M, Reynaldi A, Schlub TE, Wheatley AK, Juno JA, et al. Neutralising antibody titres as predictors of protection against SARS-CoV-2 variants and the impact of boosting: a meta-analysis. Lancet Microbe. 2022; 3(1):e52–e61. https://doi.org/10.1016/S2666-5247(21)00267-6 PMID: 34806056
3. Burton DR. Antibodies, viruses and vaccines. Nat Rev Immunol. 2002; 2(9):706–13. https://doi.org/10.1038/nri891 PMID: 12209139
4. Plotkin SA. Correlates of protection induced by vaccination. Clin Vaccine Immunol. 2010; 17(7):1055–65. https://doi.org/10.1128/CVI.00131-10 PMID: 20463105
5. Klasse PJ, Moore JP. Reappraising the Value of HIV-1 Vaccine Correlates of Protection Analyses. J Virol. 2022; 96(8):e0003422. https://doi.org/10.1128/jvi.00034-22 PMID: 35384694
6. Plotkin SA. Recent updates on correlates of vaccine-induced protection. Front Immunol. 2022; 13:1081107. https://doi.org/10.3389/fimmu.2022.1081107 PMID: 36776392
7. Burton DR. Antiviral neutralizing antibodies: from in vitro to in vivo activity. Nat Rev Immunol. 2023:1–15. https://doi.org/10.1038/s41577-023-00858-w PMID: 37069260

8. Burton DR. What Are the Most Powerful Immunogen Design Vaccine Strategies? Reverse Vaccinology 2.0 Shows Great Promise. Cold Spring Harb Perspect Biol. 2017; 9(11). https://doi.org/10.1101/cshperspect.a030262 PMID: 28159875

9. Burton DR. Advancing an HIV vaccine; advancing vaccinology. Nat Rev Immunol. 2019; 19(2):77–8. https://doi.org/10.1038/s41577-018-0103-6 PMID: 30560910

10. Haynes BF, Burton DR, Mascola JR. Multiple roles for HIV broadly neutralizing antibodies. Sci Transl Med. 2019; 11(516). https://doi.org/10.1126/scitranslmed.aaz2686 PMID: 31666399

11. Sok D, Burton DR. Recent progress in broadly neutralizing antibodies to HIV. Nat Immunol. 2018; 19 (11):1179–88. https://doi.org/10.1038/s41590-018-0235-7 PMID: 30333615

12. Escolano A, Dosenovic P, Nussenzweig MC. Progress toward active or passive HIV-1 vaccination. J Exp Med. 2017; 214(1):3–16. https://doi.org/10.1084/jem.20161765 PMID: 28003309

13. Klasse PJ, Ozorowski G, Sanders RW, Moore JP. Env Exceptionalism: Why Are HIV-1 Env Glycoproteins Atypical Immunogens? Cell Host Microbe. 2020; 27(4):507–18. https://doi.org/10.1016/j.chom.2020.03.018 PMID: 32272076

14. Klein F, Mouquet H, Dosenovic P, Scheid JF, Scharf L, Nussenzweig MC. Antibodies in HIV-1 vaccine development and therapy. Science. 2013; 341(6151):1199–204. https://doi.org/10.1126/science.1241144 PMID: 24031012

15. Kwong PD, Mascola JR. HIV-1 Vaccines Based on Antibody Identification, B Cell Ontogeny, and Epitope Structure. Immunity. 2018; 48(5):855–71. https://doi.org/10.1016/j.immuni.2018.04.029 PMID: 29768174

16. Kwong PD, Mascola JR, Nabel GJ. Broadly neutralizing antibodies and the search for an HIV-1 vaccine: the end of the beginning. Nat Rev Immunol. 2013; 13(9):693–701. https://doi.org/10.1038/nri3516 PMID: 23969737

17. Pegu A, Borate B, Huang Y, Pauthner MG, Hessell AJ, Julg B, et al. A Meta-analysis of Passive Immunization Studies Shows that Serum-Neutralizing Antibody Titer Associates with Protection against SHIV Challenge. Cell Host Microbe. 2019; 26(3):336–46 e3. https://doi.org/10.1016/j.chom.2019.08.014 PMID: 31513771

18. Caskey M. Broadly neutralizing antibodies for the treatment and prevention of HIV infection. Curr Opin HIV AIDS. 2020; 15(1):49–55. https://doi.org/10.1097/COH.0000000000000600 PMID: 31764199

19. Bar KJ, Sneller MC, Harrison LJ, Justement JS, Overton ET, Petrone ME, et al. Effect of HIV Antibody VRC01 on Viral Rebound after Treatment Interruption. N Engl J Med. 2016; 375(21):2037–50. https://doi.org/10.1056/NEJMoa1608243 PMID: 27959728

20. Halper-Stromberg A, Nussenzweig MC. Towards HIV-1 remission: potential roles for broadly neutralizing antibodies. J Clin Invest. 2016; 126(2):415–23. https://doi.org/10.1172/JCI80561 PMID: 26752643

21. Corey L, Gilbert PB, Juraska M, Montefiori DC, Morris L, Karuna ST, et al. Two Randomized Trials of Neutralizing Antibodies to Prevent HIV-1 Acquisition. N Engl J Med. 2021; 384(11):1003–14. https://doi.org/10.1056/NEJMoa2031738 PMID: 33730454

22. Gilbert PB, Huang Y, deCamp AC, Karuna S, Zhang Y, Magaret CA, et al. Neutralization titer biomarker for antibody-mediated prevention of HIV-1 acquisition. Nat Med. 2022; 28(9):1924–32. https://doi.org/10.1038/s41591-022-01953-6 PMID: 35995954

23. Wagh K, Seaman MS, Zingg M, Fitzsimons T, Barouch DH, Burton DR, et al. Potential of conventional & bispecific broadly neutralizing antibodies for prevention of HIV-1 subtype A, C & D infections. PLoS Pathog. 2018; 14(3):e1006860.

24. Burton DR, Saphire EO, Parren PW. A model for neutralization of viruses based on antibody coating of the virion surface. Curr Top Microbiol Immunol. 2001; 260:109–43. https://doi.org/10.1007/978-3-662-05783-4_7 PMID: 11443871

25. Burnet FM, Keogh EV, Lush D. The immunological reactions of the filterable viruses. Austral J Exp Biol and Med Science. 1937; 15:227–368.

26. Dulbecco R, Vogt M, Strickland AG. A study of the basic aspects of neutralization of two animal viruses, western equine encephalitis virus and poliomyelitis virus. Virology. 1956; 2(2):162–205. https://doi.org/10.1016/0042-6822(56)90017-4 PMID: 13312221

27. Iorio RM, Bratt MA. Neutralization of Newcastle disease virus by monoclonal antibodies to the hemagglutinin-neuraminidase glycoprotein: requirement for antibodies to four sites for complete neutralization. J Virol. 1984; 51(2):445–51. https://doi.org/10.1128/JVI.51.2.445-451.1984 PMID: 6205169

28. Mandel B. Neutralization of animal viruses. Adv Virus Res. 1978; 23:205–68. https://doi.org/10.1016/s0065-3527(08)60101-3 PMID: 107731

29. Ketas TJ, Holuigue S, Matthews K, Moore JP, Klasse PJ. Env-glycoprotein heterogeneity as a source of apparent synergy and enhanced cooperativity in inhibition of HIV-1 infection by neutralizing

antibodies and entry inhibitors. Virology. 2012; 422(1):22–36. https://doi.org/10.1016/j.virol.2011.09.019 PMID: 22018634

30. Alexander MR, Sanders RW, Moore JP, Klasse PJ. Short Communication: Virion Aggregation by Neutralizing and Nonneutralizing Antibodies to the HIV-1 Envelope Glycoprotein. AIDS Res Hum Retroviruses. 2015; 31(11):1160–5. https://doi.org/10.1089/AID.2015.0050 PMID: 26086186

31. Burnet FM. Immunological Studies with the Virus of Infectious Laryngotracheitis of Fowls Using the Developing Egg Technique. J Exp Med. 1936; 63(5):685–701. https://doi.org/10.1084/jem.63.5.685 PMID: 19870497

32. Hashimoto N, Prince AM. Kinetic studies on the neutralization reaction between Japanese encephalitis virus and antiserum. Virology. 1963; 19:261–72. https://doi.org/10.1016/0042-6822(63)90063-1 PMID: 13960860

33. Kjellen L. A hypothesis accounting for the effect of the host cell on neutralization-resistant virus. J Gen Virol. 1985; 66 (Pt 10):2279–83. https://doi.org/10.1099/0022-1317-66-10-2279 PMID: 2995563

34. McEwan WA, Hauler F, Williams CR, Bidgood SR, Mallery DL, Crowther RA, James LC. Regulation of virus neutralization and the persistent fraction by TRIM21. J Virol. 2012; 86(16):8482–91. https://doi.org/10.1128/JVI.00728-12 PMID: 22647693

35. McEwan WA, James LC. TRIM21-dependent intracellular antibody neutralization of virus infection. Prog Mol Biol Transl Sci. 2015; 129:167–87. https://doi.org/10.1016/bs.pmbts.2014.10.006 PMID: 25595804

36. Iorio RM, Bratt MA. Selection of unique antigenic variants of Newcastle disease virus with neutralizing monoclonal antibodies and anti-immunoglobulin. Proc Natl Acad Sci U S A. 1985; 82(20):7106–10. https://doi.org/10.1073/pnas.82.20.7106 PMID: 2413460

37. Colin P, Ringe RP, Yasmeen A, Ozorowski G, Ketas TJ, Lee WH, et al. Conformational antigenic heterogeneity as a cause of the persistent fraction in HIV-1 neutralization. Retrovirology. 2023; 20(1):9. https://doi.org/10.1186/s12977-023-00624-9 PMID: 37244989

38. Doores KJ, Burton DR. Variable loop glycan dependency of the broad and potent HIV-1-neutralizing antibodies PG9 and PG16. J Virol. 2010; 84(20):10510–21. https://doi.org/10.1128/JVI.00552-10 PMID: 20686044

39. Doores KJ, Kong L, Krumm SA, Le KM, Sok D, Laserson U, et al. Two classes of broadly neutralizing antibodies within a single lineage directed to the high-mannose patch of HIV envelope. J Virol. 2015; 89(2):1105–18. https://doi.org/10.1128/JVI.02905-14 PMID: 25378488

40. Falkowska E, Le KM, Ramos A, Doores KJ, Lee JH, Blattner C, et al. Broadly neutralizing HIV antibodies define a glycan-dependent epitope on the prefusion conformation of gp41 on cleaved envelope trimers. Immunity. 2014; 40(5):657–68. https://doi.org/10.1016/j.immuni.2014.04.009 PMID: 24768347

41. Gift SK, Leaman DP, Zhang L, Kim AS, Zwick MB. Functional Stability of HIV-1 Envelope Trimer Affects Accessibility to Broadly Neutralizing Antibodies at Its Apex. J Virol. 2017; 91(24). https://doi.org/10.1128/JVI.01216-17 PMID: 28978711

42. Julg B, Stephenson KE, Wagh K, Tan SC, Zash R, Walsh S, et al. Safety and antiviral activity of triple combination broadly neutralizing monoclonal antibody therapy against HIV-1: a phase 1 clinical trial. Nat Med. 2022. https://doi.org/10.1038/s41591-022-01815-1 PMID: 35551291

43. Kong L, Lee JH, Doores KJ, Murin CD, Julien JP, McBride R, et al. Supersite of immune vulnerability on the glycosylated face of HIV-1 envelope glycoprotein gp120. Nat Struct Mol Biol. 2013; 20(7):796–803. https://doi.org/10.1038/nsmb.2594 PMID: 23708606

44. McCoy LE, Falkowska E, Doores KJ, Le K, Sok D, van Gils MJ, et al. Incomplete Neutralization and Deviation from Sigmoidal Neutralization Curves for HIV Broadly Neutralizing Monoclonal Antibodies. PLoS Pathog. 2015; 11(8):e1005110. https://doi.org/10.1371/journal.ppat.1005110 PMID: 26267277

45. Pritchard LK, Spencer DI, Royle L, Vasiljevic S, Krumm SA, Doores KJ, Crispin M. Glycan Microheterogeneity at the PGT135 Antibody Recognition Site on HIV-1 gp120 Reveals a Molecular Mechanism for Neutralization Resistance. J Virol. 2015; 89(13):6952–9. https://doi.org/10.1128/JVI.00230-15 PMID: 25878100

46. Sok D, Doores KJ, Briney B, Le KM, Saye-Francisco KL, Ramos A, et al. Promiscuous glycan site recognition by antibodies to the high-mannose patch of gp120 broadens neutralization of HIV. Sci Transl Med. 2014; 6(236):236ra63. https://doi.org/10.1126/scitranslmed.3008104 PMID: 24828077

47. Walker LM, Phogat SK, Chan-Hui PY, Wagner D, Phung P, Goss JL, et al. Broad and potent neutralizing antibodies from an African donor reveal a new HIV-1 vaccine target. Science. 2009; 326 (5950):285–9. https://doi.org/10.1126/science.1178746 PMID: 19729618

48. Yasmeen A, Ringe R, Derking R, Cupo A, Julien JP, Burton DR, et al. Differential binding of neutralizing and non-neutralizing antibodies to native-like soluble HIV-1 Env trimers, uncleaved Env proteins,

and monomeric subunits. Retrovirology. 2014; 11:41. https://doi.org/10.1186/1742-4690-11-41 PMID: 24884783

49. Huang J, Kang BH, Pancera M, Lee JH, Tong T, Feng Y, et al. Broad and potent HIV-1 neutralization by a human antibody that binds the gp41-gp120 interface. Nature. 2014; 515(7525):138–42. https://doi.org/10.1038/nature13601 PMID: 25186731

50. Derking R, Allen JD, Cottrell CA, Sliepen K, Seabright GE, Lee WH, et al. Enhancing glycan occupancy of soluble HIV-1 envelope trimers to mimic the native viral spike. Cell Rep. 2021; 35(1):108933. https://doi.org/10.1016/j.celrep.2021.108933 PMID: 33826885

51. Behrens AJ, Harvey DJ, Milne E, Cupo A, Kumar A, Zitzmann N, et al. Molecular Architecture of the Cleavage-Dependent Mannose Patch on a Soluble HIV-1 Envelope Glycoprotein Trimer. J Virol. 2017; 91(2). https://doi.org/10.1128/JVI.01894-16 PMID: 27807235

52. Behrens AJ, Vasiljevic S, Pritchard LK, Harvey DJ, Andev RS, Krumm SA, et al. Composition and Antigenic Effects of Individual Glycan Sites of a Trimeric HIV-1 Envelope Glycoprotein. Cell Rep. 2016; 14 (11):2695–706. https://doi.org/10.1016/j.celrep.2016.02.058 PMID: 26972002

53. Pritchard LK, Vasiljevic S, Ozorowski G, Seabright GE, Cupo A, Ringe R, et al. Structural Constraints Determine the Glycosylation of HIV-1 Envelope Trimers. Cell Rep. 2015; 11(10):1604–13. https://doi.org/10.1016/j.celrep.2015.05.017 PMID: 26051934

54. Allen JD, Sanders RW, Doores KJ, Crispin M. Harnessing post-translational modifications for next-generation HIV immunogens. Biochem Soc Trans. 2018; 46(3):691–8. https://doi.org/10.1042/BST20170394 PMID: 29784645

55. Behrens AJ, Crispin M. Structural principles controlling HIV envelope glycosylation. Curr Opin Struct Biol. 2017; 44:125–33. https://doi.org/10.1016/j.sbi.2017.03.008 PMID: 28363124

56. Behrens AJ, Struwe WB, Crispin M. Glycosylation profiling to evaluate glycoprotein immunogens against HIV-1. Expert Rev Proteomics. 2017; 14(10):881–90. https://doi.org/10.1080/14789450.2017.1376658 PMID: 28870097

57. Seabright GE, Doores KJ, Burton DR, Crispin M. Protein and Glycan Mimicry in HIV Vaccine Design. J Mol Biol. 2019; 431(12):2223–47. https://doi.org/10.1016/j.jmb.2019.04.016 PMID: 31028779

58. Coss KP, Vasiljevic S, Pritchard LK, Krumm SA, Glaze M, Madzorera S, et al. HIV-1 Glycan Density Drives the Persistence of the Mannose Patch within an Infected Individual. J Virol. 2016; 90 (24):11132–44. https://doi.org/10.1128/JVI.01542-16 PMID: 27707925

59. Stewart-Jones GB, Soto C, Lemmin T, Chuang GY, Druz A, Kong R, et al. Trimeric HIV-1-Env Structures Define Glycan Shields from Clades A, B, and G. Cell. 2016; 165(4):813–26. https://doi.org/10.1016/j.cell.2016.04.010 PMID: 27114034

60. Berndsen ZT, Chakraborty S, Wang X, Cottrell CA, Torres JL, Diedrich JK, et al. Visualization of the HIV-1 Env glycan shield across scales. Proc Natl Acad Sci U S A. 2020; 117(45):28014–25. https://doi.org/10.1073/pnas.2000260117 PMID: 33093196

61. Cao L, Diedrich JK, Ma Y, Wang N, Pauthner M, Park SR, et al. Global site-specific analysis of glycoprotein N-glycan processing. Nat Protoc. 2018; 13(6):1196–212. https://doi.org/10.1038/nprot.2018.024 PMID: 29725121

62. Cao L, Pauthner M, Andrabi R, Rantalainen K, Berndsen Z, Diedrich JK, et al. Differential processing of HIV envelope glycans on the virus and soluble recombinant trimer. Nat Commun. 2018; 9(1):3693. https://doi.org/10.1038/s41467-018-06121-4 PMID: 30209313

63. Rodenburg CM, Li Y, Trask SA, Chen Y, Decker J, Robertson DL, et al. Near full-length clones and reference sequences for subtype C isolates of HIV type 1 from three different continents. AIDS Res Hum Retroviruses. 2001; 17(2):161–8. https://doi.org/10.1089/08892220150217247 PMID: 11177395

64. Santoro MM, Perno CF. HIV-1 Genetic Variability and Clinical Implications. ISRN Microbiol. 2013; 2013:481314. https://doi.org/10.1155/2013/481314 PMID: 23844315

65. Nkolola JP, Peng H, Settembre EC, Freeman M, Grandpre LE, Devoy C, et al. Breadth of neutralizing antibodies elicited by stable, homogeneous clade A and clade C HIV-1 gp140 envelope trimers in guinea pigs. J Virol. 2010; 84(7):3270–9. https://doi.org/10.1128/JVI.02252-09 PMID: 20053749

66. Seaman MS, Janes H, Hawkins N, Grandpre LE, Devoy C, Giri A, et al. Tiered categorization of a diverse panel of HIV-1 Env pseudoviruses for assessment of neutralizing antibodies. J Virol. 2010; 84 (3):1439–52. https://doi.org/10.1128/JVI.02108-09 PMID: 19939925

67. Ringe RP, Yasmeen A, Ozorowski G, Go EP, Pritchard LK, Guttman M, et al. Influences on the Design and Purification of Soluble, Recombinant Native-Like HIV-1 Envelope Glycoprotein Trimers. J Virol. 2015; 89(23):12189–210. https://doi.org/10.1128/JVI.01768-15 PMID: 26311893

68. Blattner C, Lee JH, Sliepen K, Derking R, Falkowska E, de la Pena AT, et al. Structural delineation of a quaternary, cleavage-dependent epitope at the gp41-gp120 interface on intact HIV-1 Env trimers. Immunity. 2014; 40(5):669–80. https://doi.org/10.1016/j.immuni.2014.04.008 PMID: 24768348

69. Lee JH, Andrabi R, Su CY, Yasmeen A, Julien JP, Kong L, et al. A Broadly Neutralizing Antibody Targets the Dynamic HIV Envelope Trimer Apex via a Long, Rigidified, and Anionic beta-Hairpin Structure. Immunity. 2017; 46(4):690–702.

70. Ringe RP, Ozorowski G, Yasmeen A, Cupo A, Cruz Portillo VM, Pugach P, et al. Improving the Expression and Purification of Soluble, Recombinant Native-Like HIV-1 Envelope Glycoprotein Trimers by Targeted Sequence Changes. J Virol. 2017; 91(12). https://doi.org/10.1128/JVI.00264-17 PMID: 28381572

71. Klasse PJ, LaBranche CC, Ketas TJ, Ozorowski G, Cupo A, Pugach P, et al. Sequential and Simultaneous Immunization of Rabbits with HIV-1 Envelope Glycoprotein SOSIP.664 Trimers from Clades A, B and C. PLoS Pathog. 2016; 12(9):e1005864. https://doi.org/10.1371/journal.ppat.1005864 PMID: 27627672

72. Schorcht A, Cottrell CA, Pugach P, Ringe RP, Han AX, Allen JD, et al. The Glycan Hole Area of HIV-1 Envelope Trimers Contributes Prominently to the Induction of Autologous Neutralization. J Virol. 2022; 96(1):e0155221. https://doi.org/10.1128/JVI.01552-21 PMID: 34669426

73. Scheid JF, Mouquet H, Ueberheide B, Diskin R, Klein F, Oliveira TY, et al. Sequence and structural convergence of broad and potent HIV antibodies that mimic CD4 binding. Science. 2011; 333 (6049):1633–7. https://doi.org/10.1126/science.1207227 PMID: 21764753

74. Cao L, Diedrich JK, Kulp DW, Pauthner M, He L, Park SR, et al. Global site-specific N-glycosylation analysis of HIV envelope glycoprotein. Nat Commun. 2017; 8:14954. https://doi.org/10.1038/ncomms14954 PMID: 28348411

75. Berenbaum MC. What is synergy? Pharmacol Rev. 1989; 41(2):93–141. PMID: 2692037

76. Greco WR, Bravo G, Parsons JC. The search for synergy: a critical review from a response surface perspective. Pharmacol Rev. 1995; 47(2):331–85. PMID: 7568331

77. Derking R, Ozorowski G, Sliepen K, Yasmeen A, Cupo A, Torres JL, et al. Comprehensive antigenic map of a cleaved soluble HIV-1 envelope trimer. PLoS Pathog. 2015; 11(3):e1004767. https://doi.org/10.1371/journal.ppat.1004767 PMID: 25807248

78. Bliss CI. The Toxicity Of Poisons Applied Jointly. Ann Appl Biol 1939; 26:585–615.

79. Klasse PJ. Modeling how many envelope glycoprotein trimers per virion participate in human immunodeficiency virus infectivity and its neutralization by antibody. Virology. 2007; 369(2):245–62. https://doi.org/10.1016/j.virol.2007.06.044 PMID: 17825343

80. Andrewes CH, Elford WJ. Observations on anti-phage sera. I: "The percentage law". Br J Exp Pathol. 1933; XIV(6):368–76.

81. Wu X, Yang ZY, Li Y, Hogerkorp CM, Schief WR, Seaman MS, et al. Rational design of envelope identifies broadly neutralizing human monoclonal antibodies to HIV-1. Science. 2010; 329(5993):856–61. https://doi.org/10.1126/science.1187659 PMID: 20616233

82. Checkley MA, Luttge BG, Freed EO. HIV-1 envelope glycoprotein biosynthesis, trafficking, and incorporation. J Mol Biol. 2011; 410(4):582–608. https://doi.org/10.1016/j.jmb.2011.04.042 PMID: 21762802

83. Freed EO. HIV-1 assembly, release and maturation. Nat Rev Microbiol. 2015; 13(8):484–96. https://doi.org/10.1038/nrmicro3490 PMID: 26119571

84. Regoes RR, Magnus C. The role of chance in primate lentiviral infectivity: from protomer to host organism. Prog Mol Biol Transl Sci. 2015; 129:327–51. https://doi.org/10.1016/bs.pmbts.2014.10.013 PMID: 25595809

85. van Gils MJ, van den Kerkhof TL, Ozorowski G, Cottrell CA, Sok D, Pauthner M, et al. An HIV-1 antibody from an elite neutralizer implicates the fusion peptide as a site of vulnerability. Nat Microbiol. 2016; 2:16199. https://doi.org/10.1038/nmicrobiol.2016.199 PMID: 27841852

86. Kong R, Xu K, Zhou T, Acharya P, Lemmin T, Liu K, et al. Fusion peptide of HIV-1 as a site of vulnerability to neutralizing antibody. Science. 2016; 352(6287):828–33. https://doi.org/10.1126/science.aae0474 PMID: 27174988

87. Sanders RW, Derking R, Cupo A, Julien JP, Yasmeen A, de Val N, et al. A next-generation cleaved, soluble HIV-1 Env trimer, BG505 SOSIP.664 gp140, expresses multiple epitopes for broadly neutralizing but not non-neutralizing antibodies. PLoS Pathog. 2013; 9(9):e1003618. https://doi.org/10.1371/journal.ppat.1003618 PMID: 24068931

88. Murin CD, Julien JP, Sok D, Stanfield RL, Khayat R, Cupo A, et al. Structure of 2G12 Fab2 in complex with soluble and fully glycosylated HIV-1 Env by negative-stain single-particle electron microscopy. J Virol. 2014; 88(17):10177–88. https://doi.org/10.1128/JVI.01229-14 PMID: 24965454

89. Scanlan CN, Pantophlet R, Wormald MR, Ollmann Saphire E, Stanfield R, Wilson IA, et al. The broadly neutralizing anti-human immunodeficiency virus type 1 antibody 2G12 recognizes a cluster of alpha1—>2 mannose residues on the outer face of gp120. J Virol. 2002; 76(14):7306–21.

90. Klein JS, Bjorkman PJ. Few and far between: how HIV may be evading antibody avidity. PLoS Pathog. 2010; 6(5):e1000908. https://doi.org/10.1371/journal.ppat.1000908 PMID: 20523901

91. Klein JS, Gnanapragasam PN, Galimidi RP, Foglesong CP, West AP Jr., Bjorkman PJ. Examination of the contributions of size and avidity to the neutralization mechanisms of the anti-HIV antibodies b12 and 4E10. Proc Natl Acad Sci U S A. 2009; 106(18):7385–90.

92. Calarese DA, Scanlan CN, Zwick MB, Deechongkit S, Mimura Y, Kunert R, et al. Antibody domain exchange is an immunological solution to carbohydrate cluster recognition. Science. 2003; 300 (5628):2065–71. https://doi.org/10.1126/science.1083182 PMID: 12829775

93. Zhou T, Georgiev I, Wu X, Yang ZY, Dai K, Finzi A, et al. Structural basis for broad and potent neutralization of HIV-1 by antibody VRC01. Science. 2010; 329(5993):811–7. https://doi.org/10.1126/science.1192819 PMID: 20616231

94. Moremen KW, Tiemeyer M, Nairn AV. Vertebrate protein glycosylation: diversity, synthesis and function. Nat Rev Mol Cell Biol. 2012; 13(7):448–62. https://doi.org/10.1038/nrm3383 PMID: 22722607

95. Kumar A, Narayanan V, Sekhar A. Characterizing Post-Translational Modifications and Their Effects on Protein Conformation Using NMR Spectroscopy. Biochemistry. 2020; 59(1):57–73. https://doi.org/10.1021/acs.biochem.9b00827 PMID: 31682116

96. Go EP, Chang Q, Liao HX, Sutherland LL, Alam SM, Haynes BF, Desaire H. Glycosylation site-specific analysis of clade C HIV-1 envelope proteins. J Proteome Res. 2009; 8(9):4231–42. https://doi.org/10.1021/pr9002728 PMID: 19610667

97. Seabright GE, Cottrell CA, van Gils MJ, D'Addabbo A, Harvey DJ, Behrens AJ, et al. Networks of HIV-1 Envelope Glycans Maintain Antibody Epitopes in the Face of Glycan Additions and Deletions. Structure. 2020; 28(8):897–909 e6. https://doi.org/10.1016/j.str.2020.04.022 PMID: 32433992

98. Weiss JN. The Hill equation revisited: uses and misuses. FASEB J. 1997; 11(11):835–41. PMID: 9285481

99. Struwe WB, Chertova E, Allen JD, Seabright GE, Watanabe Y, Harvey DJ, et al. Site-Specific Glycosylation of Virion-Derived HIV-1 Env Is Mimicked by a Soluble Trimeric Immunogen. Cell Rep. 2018; 24(8):1958–66 e5. https://doi.org/10.1016/j.celrep.2018.07.080 PMID: 30134158

100. Torrents de la Pena A, Rantalainen K, Cottrell CA, Allen JD, van Gils MJ, Torres JL, et al. Similarities and differences between native HIV-1 envelope glycoprotein trimers and stabilized soluble trimer mimetics. PLoS Pathog. 2019; 15(7):e1007920. https://doi.org/10.1371/journal.ppat.1007920 PMID: 31306470

101. Changeux JP, Edelstein S. Conformational selection or induced fit? 50 years of debate resolved. F1000 Biol Rep. 2011; 3:19.

102. Vauquelin G, Maes D. Induced fit versus conformational selection: From rate constants to fluxes. . . and back to rate constants. Pharmacol Res Perspect. 2021; 9(5):e00847.

103. Ozorowski G, Pallesen J, de Val N, Lyumkis D, Cottrell CA, Torres JL, et al. Open and closed structures reveal allostery and pliability in the HIV-1 envelope spike. Nature. 2017; 547(7663):360–3. https://doi.org/10.1038/nature23010 PMID: 28700571

104. Brouwer PJM, Antanasijevic A, Berndsen Z, Yasmeen A, Fiala B, Bijl TPL, et al. Enhancing and shaping the immunogenicity of native-like HIV-1 envelope trimers with a two-component protein nanoparticle. Nat Commun. 2019; 10(1):4272. https://doi.org/10.1038/s41467-019-12080-1 PMID: 31537780

105. Lee JH, Ozorowski G, Ward AB. Cryo-EM structure of a native, fully glycosylated, cleaved HIV-1 envelope trimer. Science. 2016; 351(6277):1043–8. https://doi.org/10.1126/science.aad2450 PMID: 26941313

106. Cale EM, Driscoll JI, Lee M, Gorman J, Zhou T, Lu M, et al. Antigenic analysis of the HIV-1 envelope trimer implies small differences between structural states 1 and 2. J Biol Chem. 2022; 298(4):101819. https://doi.org/10.1016/j.jbc.2022.101819 PMID: 35283191

107. Cale EM, Gorman J, Radakovich NA, Crooks ET, Osawa K, Tong T, et al. Virus-like Particles Identify an HIV V1V2 Apex-Binding Neutralizing Antibody that Lacks a Protruding Loop. Immunity. 2017; 46 (5):777–91 e10. https://doi.org/10.1016/j.immuni.2017.04.011 PMID: 28514685

108. Stadtmueller BM, Bridges MD, Dam KM, Lerch MT, Huey-Tubman KE, Hubbell WL, Bjorkman PJ. DEER Spectroscopy Measurements Reveal Multiple Conformations of HIV-1 SOSIP Envelopes that Show Similarities with Envelopes on Native Virions. Immunity. 2018; 49(2):235–46 e4. https://doi.org/10.1016/j.immuni.2018.06.017 PMID: 30076100

109. Wang H, Cohen AA, Galimidi RP, Gristick HB, Jensen GJ, Bjorkman PJ. Cryo-EM structure of a CD4-bound open HIV-1 envelope trimer reveals structural rearrangements of the gp120 V1V2 loop. Proc Natl Acad Sci U S A. 2016; 113(46):E7151–E8. https://doi.org/10.1073/pnas.1615939113 PMID: 27799557

110. Julien JP, Cupo A, Sok D, Stanfield RL, Lyumkis D, Deller MC, et al. Crystal structure of a soluble cleaved HIV-1 envelope trimer. Science. 2013; 342(6165):1477–83. https://doi.org/10.1126/science.1245625 PMID: 24179159

111. Lyumkis D, Julien JP, de Val N, Cupo A, Potter CS, Klasse PJ, et al. Cryo-EM structure of a fully glycosylated soluble cleaved HIV-1 envelope trimer. Science. 2013; 342(6165):1484–90. https://doi.org/10.1126/science.1245627 PMID: 24179160

112. Pancera M, Zhou T, Druz A, Georgiev IS, Soto C, Gorman J, et al. Structure and immune recognition of trimeric pre-fusion HIV-1 Env. Nature. 2014; 514(7523):455–61. https://doi.org/10.1038/nature13808 PMID: 25296255

113. Ward AB, Wilson IA. The HIV-1 envelope glycoprotein structure: nailing down a moving target. Immunol Rev. 2017; 275(1):21–32. https://doi.org/10.1111/imr.12507 PMID: 28133813

114. Brandenberg OF, Magnus C, Rusert P, Gunthard HF, Regoes RR, Trkola A. Predicting HIV-1 transmission and antibody neutralization efficacy in vivo from stoichiometric parameters. PLoS Pathog. 2017; 13(5):e1006313. https://doi.org/10.1371/journal.ppat.1006313 PMID: 28472201

115. Magnus C, Rusert P, Bonhoeffer S, Trkola A, Regoes RR. Estimating the stoichiometry of human immunodeficiency virus entry. J Virol. 2009; 83(3):1523–31. https://doi.org/10.1128/JVI.01764-08 PMID: 19019953

116. Klasse PJ, Moore JP. Quantitative model of antibody- and soluble CD4-mediated neutralization of primary isolates and T-cell line-adapted strains of human immunodeficiency virus type 1. J Virol. 1996; 70(6):3668–77. https://doi.org/10.1128/JVI.70.6.3668-3677.1996 PMID: 8648701

117. Pugach P, Ozorowski G, Cupo A, Ringe R, Yasmeen A, de Val N, et al. A native-like SOSIP.664 trimer based on an HIV-1 subtype B env gene. J Virol. 2015; 89(6):3380–95. https://doi.org/10.1128/JVI.03473-14 PMID: 25589637

118. Klasse PJ, Ketas TJ, Cottrell CA, Ozorowski G, Debnath G, Camara D, et al. Epitopes for neutralizing antibodies induced by HIV-1 envelope glycoprotein BG505 SOSIP trimers in rabbits and macaques. PLoS Pathog. 2018; 14(2):e1006913. https://doi.org/10.1371/journal.ppat.1006913 PMID: 29474444

119. Yang YR, McCoy LE, van Gils MJ, Andrabi R, Turner HL, Yuan M, et al. Autologous Antibody Responses to an HIV Envelope Glycan Hole Are Not Easily Broadened in Rabbits. J Virol. 2020; 94(7).

120. Escolano A, Gristick HB, Abernathy ME, Merkenschlager J, Gautam R, Oliveira TY, et al. Immunization expands B cells specific to HIV-1 V3 glycan in mice and macaques. Nature. 2019; 570(7762):468–73. https://doi.org/10.1038/s41586-019-1250-z PMID: 31142836

121. Gnanakaran S, Lang D, Daniels M, Bhattacharya T, Derdeyn CA, Korber B. Clade-specific differences between human immunodeficiency virus type 1 clades B and C: diversity and correlations in C3-V4 regions of gp120. J Virol. 2007; 81(9):4886–91. https://doi.org/10.1128/JVI.01954-06 PMID: 17166900

122. Greenspan NS. Cohen's Conjecture, Howard's Hypothesis, and Ptashne's Ptruth: an exploration of the relationship between affinity and specificity. Trends Immunol. 2010; 31(4):138–43. https://doi.org/10.1016/j.it.2010.01.001 PMID: 20149744

123. Hauser A, Carnell G, Held K, Sulbaran G, Tischbierek N, Rogers L, et al. Stepwise Conformational Stabilization of a HIV-1 Clade C Consensus Envelope Trimer Immunogen Impacts the Profile of Vaccine-Induced Antibody Responses. Vaccines (Basel). 2021; 9(7). https://doi.org/10.3390/vaccines9070750 PMID: 34358165

124. Hodge EA, Naika GS, Kephart SM, Nguyen A, Zhu R, Benhaim MA, et al. Structural dynamics reveal isolate-specific differences at neutralization epitopes on HIV Env. iScience. 2022; 25(6):104449. https://doi.org/10.1016/j.isci.2022.104449 PMID: 35677643

125. Kong L, Lee DE, Kadam RU, Liu T, Giang E, Nieusma T, et al. Structural flexibility at a major conserved antibody target on hepatitis C virus E2 antigen. Proc Natl Acad Sci U S A. 2016; 113(45):12768–73. https://doi.org/10.1073/pnas.1609780113 PMID: 27791120

126. Dey AK, Cupo A, Ozorowski G, Sharma VK, Behrens AJ, Go EP, et al. cGMP production and analysis of BG505 SOSIP.664, an extensively glycosylated, trimeric HIV-1 envelope glycoprotein vaccine candidate. Biotechnol Bioeng. 2018; 115(4):885–99. https://doi.org/10.1002/bit.26498 PMID: 29150937

127. Klasse PJ, Nixon DF, Moore JP. Immunogenicity of clinically relevant SARS-CoV-2 vaccines in nonhuman primates and humans. Sci Adv. 2021; 7(12). https://doi.org/10.1126/sciadv.abe8065 PMID: 33608249

128. Krammer F. SARS-CoV-2 vaccines in development. Nature. 2020; 586(7830):516–27. https://doi.org/10.1038/s41586-020-2798-3 PMID: 32967006

129. Ozdilek A, Avci FY. Glycosylation as a key parameter in the design of nucleic acid vaccines. Curr Opin Struct Biol. 2022; 73:102348. https://doi.org/10.1016/j.sbi.2022.102348 PMID: 35255387

130. Cohen YZ, Lorenzi JCC, Seaman MS, Nogueira L, Schoofs T, Krassnig L, et al. Neutralizing Activity of Broadly Neutralizing Anti-HIV-1 Antibodies against Clade B Clinical Isolates Produced in Peripheral Blood Mononuclear Cells. J Virol. 2018; 92(5). https://doi.org/10.1128/JVI.01883-17 PMID: 29237833

131. Willey RL, Shibata R, Freed EO, Cho MW, Martin MA. Differential glycosylation, virion incorporation, and sensitivity to neutralizing antibodies of human immunodeficiency virus type 1 envelope produced from infected primary T-lymphocyte and macrophage cultures. J Virol. 1996; 70(9):6431–6. https://doi.org/10.1128/JVI.70.9.6431-6436.1996 PMID: 8709276

132. Julg B, Sok D, Schmidt SD, Abbink P, Newman RM, Broge T, et al. Protective Efficacy of Broadly Neutralizing Antibodies with Incomplete Neutralization Activity against Simian-Human Immunodeficiency Virus in Rhesus Monkeys. J Virol. 2017; 91(20). https://doi.org/10.1128/JVI.01187-17 PMID: 28768869

133. Heeregrave EJ, Thomas J, van Capel TM, de Jong EC, Pollakis G, Paxton WA. Glycan dependent phenotype differences of HIV-1 generated from macrophage versus CD4(+) T helper cell populations. Front Immunol. 2023; 14:1107349. https://doi.org/10.3389/fimmu.2023.1107349 PMID: 37415979

134. Caskey M, Schoofs T, Gruell H, Settler A, Karagounis T, Kreider EF, et al. Antibody 10–1074 suppresses viremia in HIV-1-infected individuals. Nat Med. 2017; 23(2):185–91. https://doi.org/10.1038/nm.4268 PMID: 28092665

135. Mendoza P, Gruell H, Nogueira L, Pai JA, Butler AL, Millard K, et al. Combination therapy with anti-HIV-1 antibodies maintains viral suppression. Nature. 2018; 561(7724):479–84. https://doi.org/10.1038/s41586-018-0531-2 PMID: 30258136

136. Scheid JF, Horwitz JA, Bar-On Y, Kreider EF, Lu CL, Lorenzi JC, et al. HIV-1 antibody 3BNC117 suppresses viral rebound in humans during treatment interruption. Nature. 2016; 535(7613):556–60. https://doi.org/10.1038/nature18929 PMID: 27338952

137. Caskey M, Klein F, Nussenzweig MC. Broadly neutralizing anti-HIV-1 monoclonal antibodies in the clinic. Nat Med. 2019; 25(4):547–53. https://doi.org/10.1038/s41591-019-0412-8 PMID: 30936546

138. LaMont C, Otwinowski J, Vanshylla K, Gruell H, Klein F, Nourmohammad A. Design of an optimal combination therapy with broadly neutralizing antibodies to suppress HIV-1. Elife. 2022; 11. https://doi.org/10.7554/eLife.76004 PMID: 35852143

139. Wagh K, Bhattacharya T, Williamson C, Robles A, Bayne M, Garrity J, et al. Optimal Combinations of Broadly Neutralizing Antibodies for Prevention and Treatment of HIV-1 Clade C Infection. PLoS Pathog. 2016; 12(3):e1005520. https://doi.org/10.1371/journal.ppat.1005520 PMID: 27028935

140. Wagh K, Seaman MS. Divide and conquer: broadly neutralizing antibody combinations for improved HIV-1 viral coverage. Curr Opin HIV AIDS. 2023; 18(4):164–70. https://doi.org/10.1097/COH.0000000000000800 PMID: 37249911

141. Sneller MC, Blazkova J, Justement JS, Shi V, Kennedy BD, Gittens K, et al. Combination anti-HIV antibodies provide sustained virological suppression. Nature. 2022. https://doi.org/10.1038/s41586-022-04797-9 PMID: 35650437

142. Laal S, Burda S, Gorny MK, Karwowska S, Buchbinder A, Zolla-Pazner S. Synergistic neutralization of human immunodeficiency virus type 1 by combinations of human monoclonal antibodies. J Virol. 1994; 68(6):4001–8. https://doi.org/10.1128/JVI.68.6.4001-4008.1994 PMID: 7514683

143. Wei X, Decker JM, Liu H, Zhang Z, Arani RB, Kilby JM, et al. Emergence of resistant human immunodeficiency virus type 1 in patients receiving fusion inhibitor (T-20) monotherapy. Antimicrob Agents Chemother. 2002; 46(6):1896–905. https://doi.org/10.1128/AAC.46.6.1896-1905.2002 PMID: 12019106

144. Depetris RS, Julien JP, Khayat R, Lee JH, Pejchal R, Katpally U, et al. Partial enzymatic deglycosylation preserves the structure of cleaved recombinant HIV-1 envelope glycoprotein trimers. J Biol Chem. 2012; 287(29):24239–54. https://doi.org/10.1074/jbc.M112.371898 PMID: 22645128

145. Lander GC, Stagg SM, Voss NR, Cheng A, Fellmann D, Pulokas J, et al. Appion: an integrated, database-driven pipeline to facilitate EM image processing. J Struct Biol. 2009; 166(1):95–102. https://doi.org/10.1016/j.jsb.2009.01.002 PMID: 19263523

146. Cheng A, Negro C, Bruhn JF, Rice WJ, Dallakyan S, Eng ET, et al. Leginon: New features and applications. Protein Sci. 2021; 30(1):136–50. https://doi.org/10.1002/pro.3967 PMID: 33030237

147. Zheng SQ, Palovcak E, Armache JP, Verba KA, Cheng Y, Agard DA. MotionCor2: anisotropic correction of beam-induced motion for improved cryo-electron microscopy. Nat Methods. 2017; 14(4):331–2. https://doi.org/10.1038/nmeth.4193 PMID: 28250466

148. Punjani A, Rubinstein JL, Fleet DJ, Brubaker MA. cryoSPARC: algorithms for rapid unsupervised cryo-EM structure determination. Nat Methods. 2017; 14(3):290–6. https://doi.org/10.1038/nmeth.4169 PMID: 28165473

149. Zhang K. Gctf: Real-time CTF determination and correction. J Struct Biol. 2016; 193(1):1–12. https://doi.org/10.1016/j.jsb.2015.11.003 PMID: 26592709

150. Pettersen EF, Goddard TD, Huang CC, Couch GS, Greenblatt DM, Meng EC, Ferrin TE. UCSF Chimera—a visualization system for exploratory research and analysis. J Comput Chem. 2004; 25 (13):1605–12. https://doi.org/10.1002/jcc.20084 PMID: 15264254

151. Casanal A, Lohkamp B, Emsley P. Current developments in Coot for macromolecular model building of Electron Cryo-microscopy and Crystallographic Data. Protein Sci. 2020; 29(4):1069–78. https://doi.org/10.1002/pro.3791 PMID: 31730249

152. Afonine PV, Poon BK, Read RJ, Sobolev OV, Terwilliger TC, Urzhumtsev A, Adams PD. Real-space refinement in PHENIX for cryo-EM and crystallography. Acta Crystallogr D Struct Biol. 2018; 74(Pt 6):531–44. https://doi.org/10.1107/S2059798318006551 PMID: 29872004

153. Conway P, Tyka MD, DiMaio F, Konerding DE, Baker D. Relaxation of backbone bond geometry improves protein energy landscape modeling. Protein Sci. 2014; 23(1):47–55. https://doi.org/10.1002/pro.2389 PMID: 24265211

154. Williams CJ, Headd JJ, Moriarty NW, Prisant MG, Videau LL, Deis LN, et al. MolProbity: More and better reference data for improved all-atom structure validation. Protein Sci. 2018; 27(1):293–315. https://doi.org/10.1002/pro.3330 PMID: 29067766

155. Barad BA, Echols N, Wang RY, Cheng Y, DiMaio F, Adams PD, Fraser JS. EMRinger: side chain-directed model and map validation for 3D cryo-electron microscopy. Nat Methods. 2015; 12(10):943–6. https://doi.org/10.1038/nmeth.3541 PMID: 26280328

156. Ringe RP, Cruz Portillo VM, Dosenovic P, Ketas TJ, Ozorowski G, Nogal B, et al. Neutralizing Antibody Induction by HIV-1 Envelope Glycoprotein SOSIP Trimers on Iron Oxide Nanoparticles May Be Impaired by Mannose Binding Lectin. J Virol. 2020; 94(6). https://doi.org/10.1128/JVI.01883-19 PMID: 31852794

157. Walker LM, Huber M, Doores KJ, Falkowska E, Pejchal R, Julien JP, et al. Broad neutralization coverage of HIV by multiple highly potent antibodies. Nature. 2011; 477(7365):466–70. https://doi.org/10.1038/nature10373 PMID: 21849977

158. Trkola A, Purtscher M, Muster T, Ballaun C, Buchacher A, Sullivan N, et al. Human monoclonal antibody 2G12 defines a distinctive neutralization epitope on the gp120 glycoprotein of human immunodeficiency virus type 1. J Virol. 1996; 70(2):1100–8. https://doi.org/10.1128/JVI.70.2.1100-1108.1996 PMID: 8551569

159. Huang J, Ofek G, Laub L, Louder MK, Doria-Rose NA, Longo NS, et al. Broad and potent neutralization of HIV-1 by a gp41-specific human antibody. Nature. 2012; 491(7424):406–12. https://doi.org/10.1038/nature11544 PMID: 23151583